Università degli Studi di Napoli Federico II

Facoltà di Ingegneria

Dipartimento di Ingegneria Chimica, dei Materiali e della Produzione Industriale

Tesi di Dottorato in Ingegneria dei Materiali e delle Strutture (XXVII ciclo)

Dynamic Topographic Patterns to Control Cell Adhesion and Mechanics

Carmela Rianna

Relatore

Prof. Paolo A. Netti

Coordinatore

Prof. Giuseppe Mensitieri

Correlatori

Prof. Maurizio Ventre

Dr. Silvia Cavalli

Marzo 2012 – Marzo 2015

DYNAMIC TOPOGRAPHIC PATTERNS TO CONTROL CELL ADHESION AND MECHANICS

A THESIS SUBMITTED IN PARTIAL FULFILMENT OF THE REQUIREMENT FOR THE DEGREE OF DOCTOR OF PHILOSOPHY IN
MATERIALS AND STRUCTURES ENGINEERING

AUTHOR
Carmela Rianna

ADVISOR
Prof. Dr. Paolo A. Netti

TUTORS
Prof. Dr. Maurizio Ventre
Dr. Silvia Cavalli

COORDINATOR
Prof. Dr. Giuseppe Mensitieri

COLLABORATIONS
Prof. Dr. Pietro Ferraro, CNR − Istituto di Cibernetica, Pozzuoli, Naples, Italy
Prof. Dr. Manfred Radmacher, Institute for Biophysics, Bremen, Germany

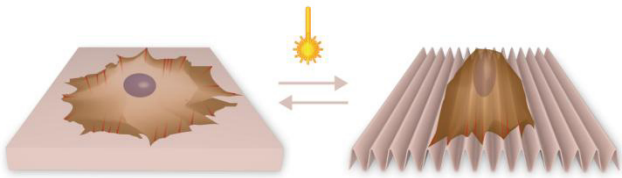

Table of Contents

Chapter 1

Introduction 9

1.1 Tissue Engineering 10
1.2 Cell−Material Interaction 11
1.2.1. Cell−Topography Crosstalk 14
1.2.2. Dynamic Topographic Signals 17
1.2.3. Cell Mechanics 18
1.3 Azopolymers 20
1.3.1. Azobenzene Cromophores 21
1.3.2. Photoinduced Azobenzene Motions 23
1.3.3. Surface Relief Gratings 25
1.3.4. Azopolymers for Biological Applications 28
1.4 Aim and Outline of the Thesis 28
1.5 References 31

Chapter 2

Reversible Holographic Patterns on Azopolymers for Guiding Cell Adhesion and Orientation 37

2.1 Introduction 38
2.2 Materials and Methods 40
2.2.1 SRG Realization and Erasure 41

2.2.2 Cell Culture and Immunofluorescence 42
2.3 Results and Discussion 44
2.3.1 Cell Adhesion, Orientation and Elongation 47
2.3.2 SRG Reversibility Tests 52
2.4 Conclusions 59
2.5 References 60

Chapter 3

Cell Mechanics Investigation on Patterned Azopolymers by Using AFM Technique 63

3.1 Introduction 64
3.2 Materials and Methods 66
3.2.1 Detecting Cell Mechanical Properties by AFM 66
3.2.2 Cell Culture and Staining Procedures 67
3.3 Results and Discussion 68
3.3.1 Analysis of Mechanical Proprieties on Several Cell Regions 69
3.3.2 Comparing Cell Mechanical Properties to Cell Height 72
3.3.3 Cell Nuclei Morphology and Cytoskeleton Organization 76
3.4 Conclusions 85
3.5 References 86

Chapter 4

Pattern Inscription on Azopolymers by Confocal Microscopy Technique: an in Vitro Approach for Dynamic Cell Guidance 91

4.1 Introduction 92
4.2 Materials and Methods 94
4.2.1 Pattern Realization 94
4.2.2 Replica Molding Technique 95
4.2.3 Cell Culture Experiments 96
4.3 Results and Discussion 97
4.3.1 Relation between Microscope Parameters and Pattern Features 99
4.3.2 PDMS and NOA63 Replica Molding 103
4.3.3 Cell Behavior on Geometrical Patterns 105
4.3.4 Real−Time Dynamic Cell Guidance 106
4.4 Conclusions 110
4.5 References 112

Conclusions and Future Prospects 115

List of Publications 119

Appendix: Influence of Material Stiffness on Cell Mechanics 121

Acknowledgments **127**

Chapter 1

Introduction

Abstract. Understanding cellular reaction and response to the external environment is a central aspect in tissue engineering and biomedical science. A growing number of works is emphasizing the high sensitivity that cells display towards the chemical and physical features of the substrate which they are connected to. In particular, substrates of defined topographies have emerged as powerful tools in the investigation of these mechanisms. The limitation of many of the proposed substrates is their static form that does not allow to induce a programmed change during cell culture. This physical stasis has limited the potential of topographic substrates to control cells in culture. In this thesis a study on dynamic and reversible platforms is reported, aiming to investigate cell behavior in a more bio−mimetic way and to overcome the limit of static systems. In the first part of the introduction the main aspects involved in cell−material interaction are discussed. The second part is mainly focused on azopolymers, which have been used as dynamic platforms in cell culture to study cell adhesion and mechanics.

1.1 Tissue Engineering

Tissue engineering refers to the practice of combining scaffolds, cells and biologically active molecules into functional tissues. The goal of tissue engineering is to assemble functional constructs that restore, maintain, or improve damaged tissues or whole organs.[1,2] The ability of an engineered biomaterial to approximate the structural and mechanical aspects of the cellular microenvironment is an important factor in determining the success or failure of engineered devices for tissue repair or replacement. Biological tissues basically consist of cells, signaling systems and extracellular matrix (ECM).[3] The cells are the core of the tissue, however, in the absence of signaling systems and/or of the ECM cannot explicate their functions. In fact, cells are the building blocks of tissue, and tissues are the basic unit of function in the body. Generally, groups of cells make and secrete their own supporting structures, that is the extracellular matrix.[4] This matrix, or scaffold, does more than just support the cells; it also acts as a relay station for various signaling molecules. Thus, cells receive messages from many sources that become available from the local environment. Each signal can elicit a cascade of responses that determine what happens to the cell. By understanding how cells respond to signals, interact with their environment and organize into tissues and organisms, many researchers were able to manipulate these processes to mend damaged tissues or even create new ones. When engineering and designing a new biomaterial, one of the most important aspect that have to be largely considered is the interaction between cells and material surface, namely cell−material interaction.

1.2 Cell−Material Interaction

Cell−material interaction occurs through a combination of biochemical and biophysical signals, including interfacial presentation of molecular, topographic and mechanical cues. Indeed, both biochemical and biophysical features of the biomaterial have been reported to affect and influence cell functions by triggering specific molecular events at the cell−material interface. Cellular activities that are mostly influenced by material properties are adhesion, spreading, migration, proliferation and differentiation.[5] Cell adhesion and migration are highly complex and multistep processes, which share many common features. They both involve several compartments of the cell, including surface receptors, signaling elements and the cytoskeleton, which is a cellular structure mainly responsible for dictating cell shape and tissue elasticity (Figure 1.1).[6] Both processes involve actin filaments. These are components of the cytoskeleton, a composite filamentous structure that influences cell shape and cell contractility on the cellular scale. Actin filaments are distributed throughout the cell and give the appearance of a gel network. Some molecular motors, such as Myosin II, can contribute as active cross−linkers. Energetically driven changes of conformation of the molecular motors make actin polymer chains slide respective to the others.

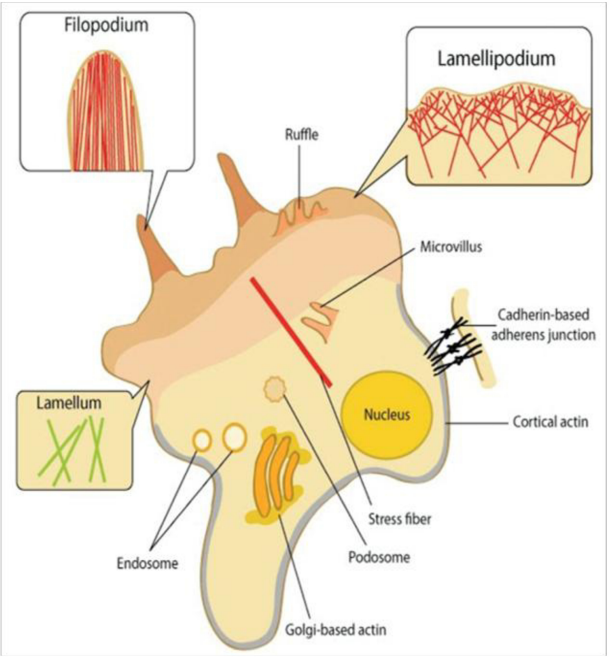

Figure 1.1. Schematic representation of the different actin cytoskeleton assemblies within cells.

The collective contribution of the molecular motors leads to a global contraction of the network.[7] Contracting bundles of actin play a dominant role in the cellular adhesion machinery and are named stress fibers as a consequence of their morphology.[8] Actin cytoskeleton is intrinsically mechanosensitive, in the sense that it adapts to mechanical forces. Connection of the actin cytoskeleton to clusters of proteins that are anchored to the ECM makes it suitable to probe the mechanical properties of the extracellular environment, as a response to the resistance that adhesion−mediated anchorage makes to its contraction. The signaling pathways that coordinate the formation of new adhesions

as well as their maturation, are intimately linked to the dynamical reorganization of the actin cytoskeleton.[9]

Focal adhesions (FAs) are sites of tight adhesion to the underlying ECM developed by cells in culture during their adhesion. As such, they constitute a structural link between the actin cytoskeleton and the ECM and are regions of signal transduction between the outside environment and the inside cellular cytoplasm. In Figure 1.2 a single FA is presented.

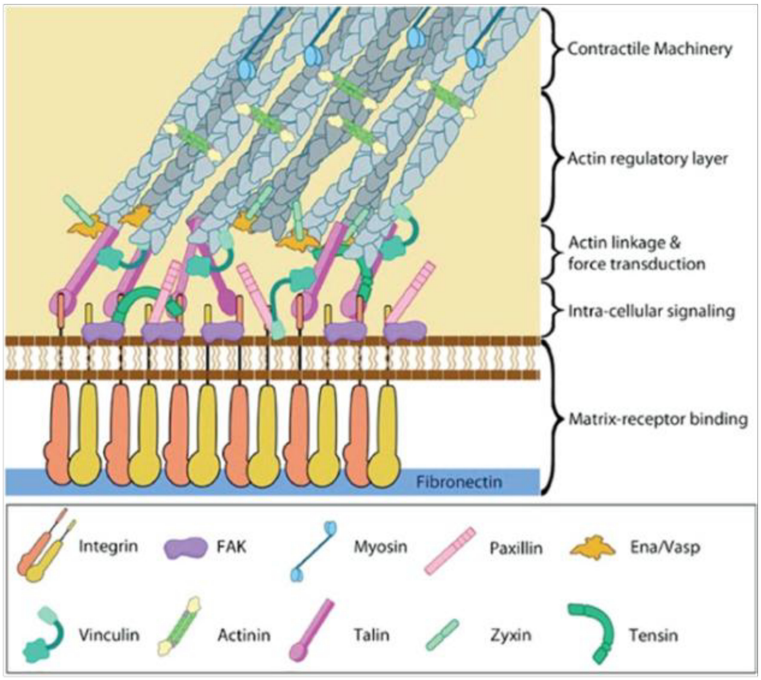

Figure 1.2. Schematic representation of a single FA.

A mature FA contains hundreds of proteins that are grouped based on their contribution to four basic processes: receptor/matrix binding, linkage to actin cytoskeleton, intracellular signal transduction and actin

polymerization. Both actin polymerization and acto−myosin contractile machinery generate forces that affect mechanosensitive proteins in the actin linking module, the receptor module (e.g. integrins), the signaling module and the actin polymerization module. The combined activity of the mechanosensitive components forms the mechanoresponsive network.

1.2.1 Cell−Topography Crosstalk

In in−vivo contexts, extracellular environment represents a set of topographic signals, perceived by cells at different length scale. Fibrils and fiber bundles (collagen and fibrin), rough surfaces (crystal deposit in bone) and porous membranes (basement membranes) represent examples of natural topographies. These topographical signals play a relevant role in cell−material interaction through direct alteration in several cellular processes.[10] Recent advancements in micro− and nano−fabrication technologies made it possible to imprint on substrate surfaces topographic features favoring the study of the role of topography in cell–material interaction. Soft lithography,[11,12] electron beam lithography[13] and nano−imprint lithography[14] can emboss topographic patterns with a tightly controlled spatial resolution (of a few nanometers). Cells interact with native topographical structures in many ways, often through a phenomenon known as contact guidance. Contact guidance is a leading example of a naturally occurring phenomenon that is characterized by the response of cells to structures on the micron and sub−micron scale.[15] Cell−nanotopography interactions can induce different effects within a single cell type due to

the coupled effect of nanotopography in combination with physicochemical properties of the substrate. These interactions also vary across cell type, feature size, and feature geometry as well. Nevertheless, there are some general trends that can be extricated from the rapidly growing body of literature.[16] Cells respond to two−dimensional synthetic topographic substrates in a wide array of responses, which depend upon many factors including cell type, feature size and geometry[17] or the physical properties of the bulk substrate material including substrate stiffness.[18] For example, Bettinger et al.[16] reported epithelial cell response to nano−topography (Figure 1.3).

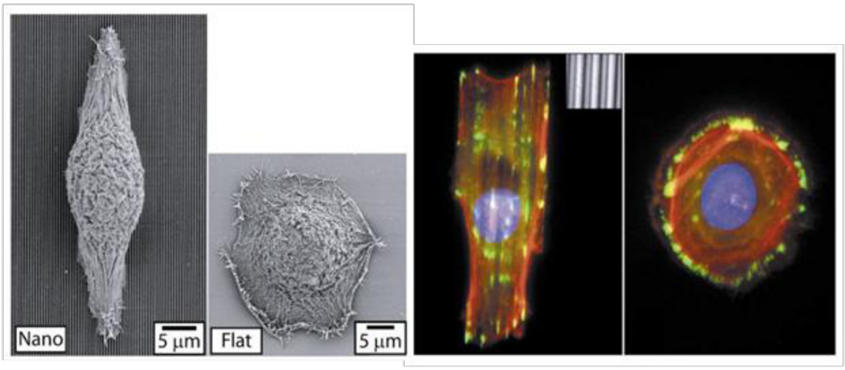

Figure 1.3. Cell−Nanograting response in epithelial cells. Epithelial cells respond to nanograting through alignment and elongation to the grating axis as evident through fluorescent and SEM micrographs.[16]

Furthermore, Walboomers et al.[15] reported the behavior of fibroblasts cultured on a grooved polystyrene substratum (Figure 1.4) and hypothesized that micro−grooves created a pattern of mechanical stress, which influenced cell spreading and caused the cell to be aligned with surface microgrooves. Also smooth muscle cells showed

to be influenced by nano−topography imprinted on polydimethylsiloxane (PDMS) and polymethylmethacrylate (PMMA), as reported in Figure 1.5.[19] Therefore, in all these examples cell behavior on nanotopography was similar even if cell type was different.

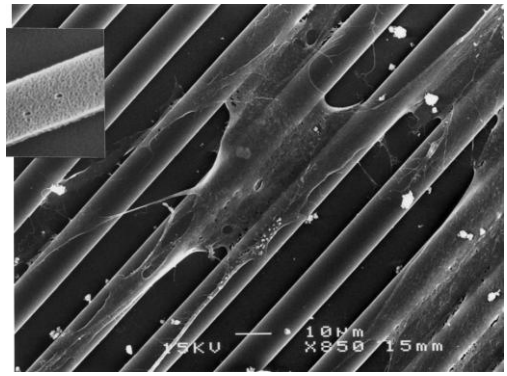

Figure 1.4. Scanning electron micrograph, showing a rat dermal fibroblast on a 10 μm wide−grooved polystyrene substrate.[15]

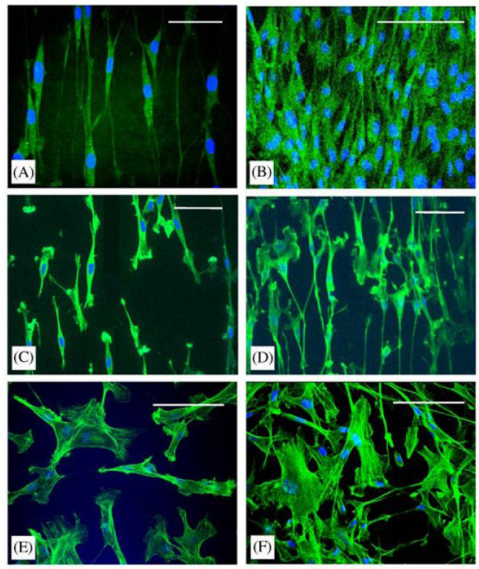

Figure 1.5. Confocal micrographs of actin stained smooth muscle cells on (A) nano−imprinted PMMA at low cell density, (B) nano−imprinted PMMA at high cell density, (C) nanopatterned PDMS at low cell density, (D)

nano−patterned PDMS at high cell density, (E) non−patterned PMMA and (F) glass cover slip. Scale bar are 50 µm for all except (B) scale bar is100 µm.[19]

1.2.2 Dynamic Topographic Signals

Several techniques have been proposed to encode micro− and nano−topographies on material surfaces, in order to investigate many processes involved in cell−material interaction. Despite possessing a very high spatial resolution, these techniques require expensive equipments and are time consuming. Additionally, once produced, the geometric features of the master or substrate cannot be readily modified *a posteriori* since they are intrinsically static in nature. In order to overcome the limits of a physically static system and to develop more versatile platforms, large interest has recently arisen in using stimuli−responsive materials as dynamic supports to investigate cell response. For example, Davis et al.[20] have proposed a thermo−responsive cell culture system, used to control cell behavior via surface shape memory polymers (Figure 1.6).

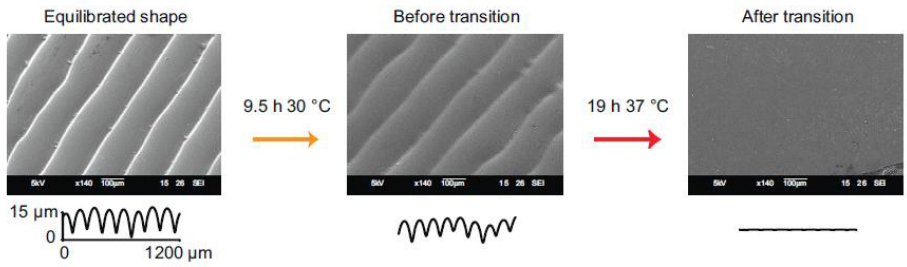

Figure 1.6. Active cell culture substrate transitions from a grooved topography to a flat surface.[20]

In details, by taking advantage of a polymer with a glass transition temperature of 37°C, the temporary patterned shape could be switched in the flat stable form during cell culture. Among all the stimuli−responsive materials, this thesis focuses on photo−switchable polymers, aiming to control the topographic surface with light as external stimulus in a precise way. Azopolymers were selected as the best candidate, aiming to realize dynamic supports for studying cell adhesion and mechanics (see paragraph 1.3 for more details).

1.2.3 Cell Mechanics

Physical cues like surface topography, surface mechanics, or external forces play a fundamental role in a wide range of biological processes. One of the most prominent properties reflecting cell response to the environment is cell mechanics. Using cell mechanics in diverse bioengineering and clinical areas is a continuously growing field. In fact, in the last years, cell mechanics investigation has proven to be a promising tool for clinical and medical applications, such as cancer diagnostics[21–23] or tissue engineering, where cell mechanical properties can be quantitative markers, monitoring the regulation of cell differentiation.[24–26] Cell mechanics can be evaluated with several methods, such as micropipette aspiration,[27] optical tweezers,[28] magnetic twisting cytometry[29] and atomic force microscopy (AFM).[30] Among these, AFM is the most widely used technique for adherent cells, allowing both imaging and mechanical properties quantification of heterogeneous living samples, such as cells. Since its invention, almost 30 years ago,[31] the AFM has become an important tool for

studying surface and mechanical properties very first of hard samples, but soon its potential for soft and biological samples was discovered.[32–34] By obtaining force–distance AFM curves (Figure 1.7), cell elastic properties can be measured in terms of elastic or Young's modulus.[30,35]

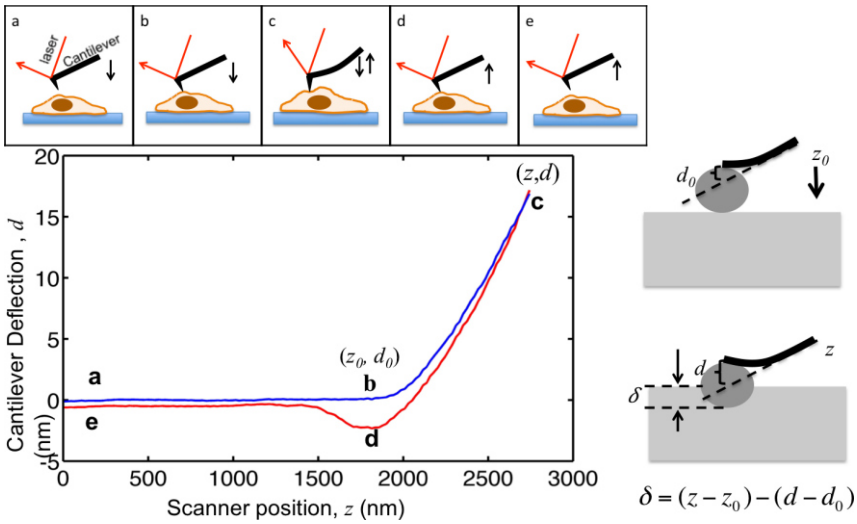

Figure 1.7. The top panel shows the motion of AFM cantilever driven by the piezo scanner. The vertical location of cantilever z and the cantilever deflection signal d is recorded during the process. The cantilever starts from point a, a few micrometers above the cell. While approaching the cell, the sample indentation δ remains zero until it reaches point b, where the tip comes into contact with the cell. The coordinates of point b in the plot are critical values for data analysis, denoted by (z_0, d_0). From b to c, the cantilever indents into the cell until the cantilever deflection reaches a set point, which is set to be the ratio between the targeted maximum indenting force and the cantilever spring constant. Once the deflection signal reaches the preset maximum value, the cantilever is then withdrawn from the cell to point d, where it often be pulled downwards due to tip–sample adhesion, detaches from the cell and returns to its initial location at e. The right panel illustrates the relationship between the indentation and the recorded z and d signal. The lower left panel is a plot of a representative force curve.[35]

In order to understand the interaction between ECM signals and cell mechanics, several studies have been performed. For example it has been shown that cell spreading and stiffness directly depend on mechanical properties of the underlying materials.[36,37] In this thesis the effect of mechanical and topographic signals on cell mechanics was investigated (See "Appendix: Influence of Material Stiffness on Cell Mechanics" and Chapter 3, for cell mechanics investigation on different topographic patterns).

1.3 Azopolymers

The study presented here is based on the use of azopolymers as dynamic and light−switchable supports for cell culture.

Azopolymers consist of polymers functionalized with azobenzene molecules. Owing to the intrinsic properties of azobenzene moieties, azopolymers belong to a class of light−responsive materials. In fact, the photoisomerization reaction of azobenzene molecules can induce reversible material motions at molecular, mesoscopic, and even macroscopic length scales. Amorphous azopolymer films can form stable surface relief patterns upon exposure to interfering light. This allows obtaining periodic micro− and nano−structures in a remarkably simple way.

Following it is reported a description of azobenzene chromophores, their motions at different scales, surface relief grating fabrication and application of azopolymers for biological applications.

1.3.1 Azobenzene Cromophores

Azobenzene is an aromatic molecule formed by an azo linkage (–N=N–) connecting two phenyl rings. Originally, azobenzenes were used as dyes and colorants, due to their powerful colors.[38] At a later stage, their amazing properties were discovered and exploited in many field. The most fascinating characteristic of the azobenzenes is their reversible photoisomerization. Azobenzenes have two stable isomeric states: a thermally stable *trans* configuration and a metastable *cis* form (Figure 1.8). Remarkably, the azobenzene chromophore can interconvert between these isomers upon absorption of a photon. For most azobenzenes, the molecule can be optically isomerized from *trans* to *cis* with light and the molecule will subsequently thermally relax back to the *trans* state on a timescale dictated by the substitution pattern. This photochemistry is central to azobenzene potential use as a tool for nanopatterning.

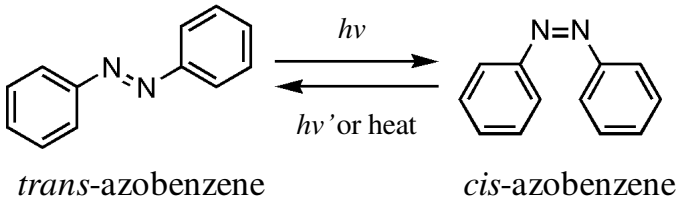

Figure 1.8. Azobenzene photoisomerization. The *trans* form (left) can be converted to the *cis* form (right) using an appropriate wavelength of light. A different wavelength will induce the molecule back conversion to the *trans* form. Alternately, the molecule will thermally relax to the stable *trans* form.

Azobenzenes can be separated into three spectroscopic classes: azobenzene−type, aminoazobenzene−type, and pseudo−stilbenes molecules (Figure 1.9).[39]

The azobenzene−type molecules have a strong absorption in the UV, and a low−intensity band in the visible. The aminoazobenzenes and pseudo−stilbenes typically have strong overlapped absorptions in the visible region. The photoisomerization between *trans* (E) and *cis* (Z) isomers is completely reversible and free from side reactions, such that it is characterized as one of the cleanest photoreactions known.[39] In the dark, most azobenzene molecules will be found in the *trans* form.

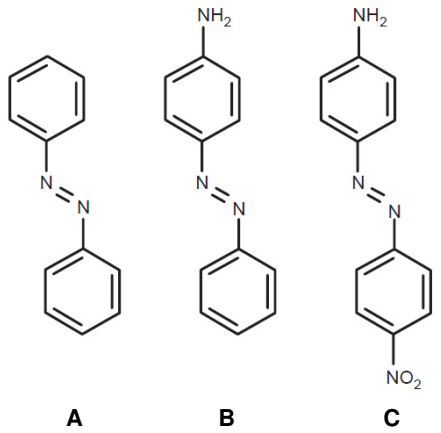

Figure 1.9. Examples of azobenzene molecules. (A) Azobenzenes, (B) aminoazobenzenes and (C) pseudo−stilbenes.

Upon absorption of a photon (with a wavelength in the *trans* absorption band), the azobenzene will convert, with high efficiency, into the *cis* isomer. A second wavelength of light (corresponding to the *cis* absorption band) can cause the back−conversion. These photoisomerizations usually have picosecond timescales.[40] Alternately,

azobenzenes will thermally reconvert from the *cis* to *trans* state, with a timescale ranging from milliseconds to hours, depending on the substitution pattern and local environment. In some cases, bulky substituents can inhibit the *cis* → *trans* relaxation process, thereby allowing the *cis* state to persist for days.[41]

1.3.2 Photoinduced Azobenzene Motions

Irradiation with light produces molecular changes in azobenzenes, and under appropriate conditions, these changes can translate into larger scale motions and even modulation of material properties. Molecular motions, photo orientation and consequent birefringence and macroscopic motions are some of the molecule movements that occur under irradiation. The fundamental molecular photo−motion in azobenzenes is the geometrical change that occurs upon absorption of light. The geometrical changes in azobenzene are very large, by molecular standards, and it is thus no surprise that isomerization modifies a wide host of material properties. This molecular displacement generates a nanoscale force, which has been measured in single molecule force spectroscopy experiments.[42] In these experiments, illumination causes contraction of an azobenzene polymer, showing that each chromophore can exert pN molecular forces on−demand.

Additionally, orientation of azobenzene chromophores can be manipulated using polarized light (Figure 1.10). Azobenzenes preferentially absorb light polarized along their transition dipole axis (long axis of the azobenzene molecule). The probability of absorption

varies as $\cos^2 \phi$, where ϕ is the angle between the light polarization and the azobenzene dipole axis. Thus, azomolecules oriented along the polarization of the light will absorb, whereas those oriented against the light polarization will not. For a given initial angular distribution of chromophores, many will absorb, convert into the *cis* form, and then revert to the *trans* form with a new random direction. Those chromophores that fall perpendicular to the light polarization will no longer isomerize and reorient; hence, there is a net depletion of chromophores aligned with the light polarization, with a concomitant increase in the population of chromophores aligned perpendicular (i.e., orientation hole burning).

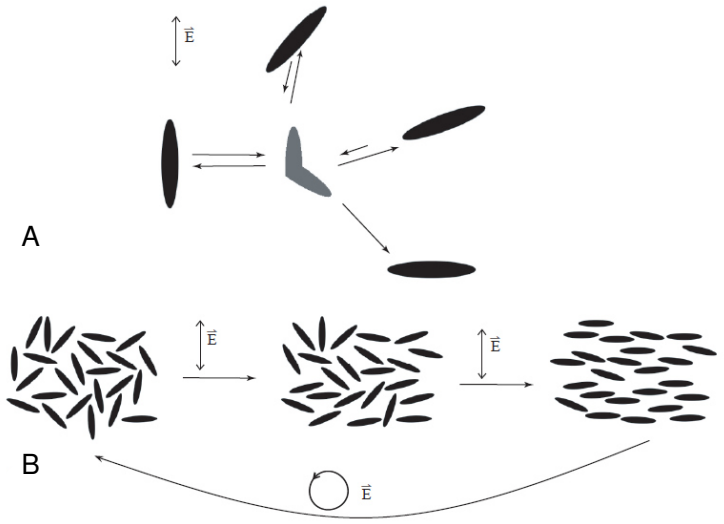

Figure 1.10. Statistical photo−orientation of azobenzene molecules. (A) The molecules aligned along the polarization direction of the incident light absorb, isomerize, and re−orient. Those aligned perpendicular cannot absorb and remain fixed. (B) Irradiation of an isotropic samples leads to accumulation of chromophores in the perpendicular direction. Circularly polarized light restores isotropy.

This statistical reorientation is fast, and gives rise to strong birefringence (anisotropy in refractive index) and dichroism (anisotropy in absorption spectrum) due to the large anisotropy of the azo electronic system. Because unpolarized light can photo−orient (along the axis of illumination), even sunlight is suitable. [43]

1.3.3 Surface Relief Gratings

Along the line of active cell culture substrates, holographic imprinting of surface relief gratings (SRGs) on azopolymer films is a promising approach for a straightforward fabrication of dynamic substrates. Large−scale surface mass displacement was observed by Natansohn and Kumar groups who irradiated azopolymer films with an interference pattern of light.[44,45] Once the sinusoidal pattern of light is in contact with the polymer, it is able to induce the formation of SRGs, in the form of topographic arrays that trace out the light intensity profile. This phenomenon has been used to realize micro− and nano−grooved polymer films, suitable in many applications, such as optics and photonics.[46,47]

In a typical experiment, two coherent laser beams, with a wavelength in the azobenzene absorption band, are intersected at the sample surface (Figure 1.11). The sample usually consists of a thin spin−cast film (10–1000 nm) of an amorphous azo−polymer on a transparent substrate.

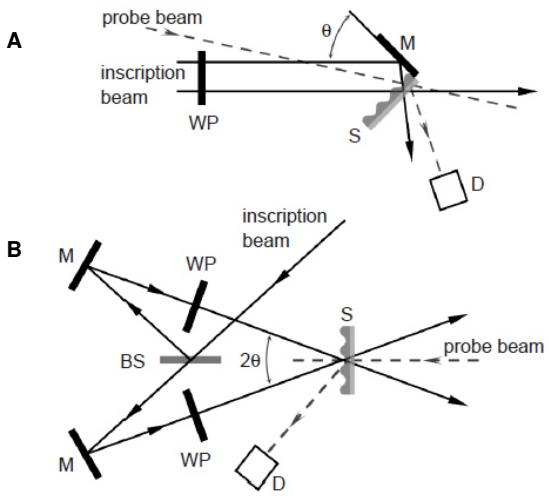

Figure 1.11. Experimental setup for the inscription of a surface relief grating: S refers to the sample, M are mirrors, D is a detector for the diffraction of the probe beam, WP is a waveplate (or generally a combination of polarizing elements), and BS is a 50% beam splitter. (A) A simple one−beam inscription involves reflecting half of the incident beam off of a mirror adjacent to the sample. (B) A two−beam interference setup enables independent manipulation of the polarization state of the two incident beams.

The sinusoidal light interference pattern at the sample surface leads to a sinusoidal surface patterning, i.e. SRG. The process occurs readily at room temperature (well below the T_g of the amorphous polymers used) with moderate irradiation (1–100 mW/cm^2) over seconds to minutes. The phenomenon is a reversible mass transport, not irreversible material ablation, since a flat film with the original thickness is recovered upon heating above T_g. Upon irradiation with linearly polarized light of appropriate wavelength, the azobenzene molecules statistically reorient and accumulate to the direction perpendicular to the polarization plane (Figure 1.12). The resulting molecular alignment

gives rise to optical anisotropy that can be erased by irradiating the sample with circularly polarized or unpolarized light.[48,49]

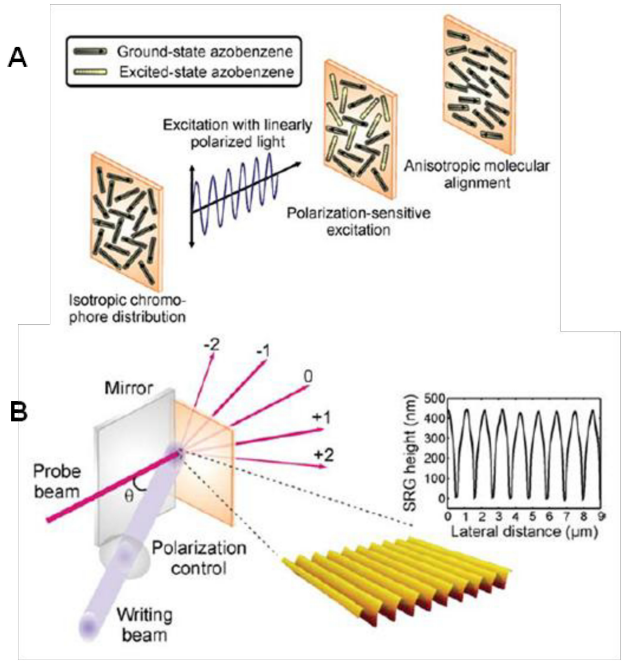

Figure 1.12. (A) Schematic illustration of the photoalignment of azobenzenes with polarized light. (B) Representation of the SRG inscription process. An atomic force micrograph and a surface profile of an inscribed grating are shown on the right.

When a thin amorphous azopolymer film is irradiated with an optical interference pattern, the material starts to migrate and move away from high−intensity areas to form a replica of the incident irradiation in the form of a SRG. Many models have been proposed to explain this mechanism, such us thermal model,[50] pressure gradient force model,[51] mean−field model,[52] optical−field gradient force model.[53,54] However a controversy regarding the mechanism still remains.

1.3.4 Azopolymers for Biological Applications

The phenomenon of SRG inscription on azopolymers has been used to realize micro− and nano−grooved polymer films, suitable in many applications, such as optics and photonics.[46,47] Despite their extraordinary chemical/physical characteristics the number of studies on the use of azobenzene−based substrates for cell cultures is very limited. However some examples are reported here. For instance, Baac et al.[55] used SRGs as cell supports for controlling cell growth, adhesion and orientation. They found that human astrocytes were highly oriented along the groove direction.

Moreover, Rocha et al.[56] studied the biocompatibility of azopolymers based polysiloxane coatings and investigated the stability of the substrates in aqueous environment.

Barille et al.[57] examined the imprinting capabilities of the azo−based photo−switchable materials both in dry and wet conditions and analyzed neuron response to the topographic signal.

However, the possibility to exploit writing/erasing reversibility of azobenzene polymers in biological applications has not been addressed yet. This aspect has been investigated in this thesis.

1.4 Aim and Outline of the Thesis

The main aim of the thesis is to realize dynamic supports for cell culture in order to study and guide cell adhesion and mechanics in a non−static and biomimetic way. As a matter of fact, topography has shown to influence cell behavior in many processes, such as migration, orientation, differentiation, mechanics. Despite many techniques have

been proposed to realize micro− and nano−patterns on material surface, many of them are based on static substrates, which do not allow to change their shape once cells are seeded on them. In Nature, cells are subjected to continuous modifications of the local environment and are constantly changing their behavior accordingly. Therefore, in order to overcome the limits of a physically static system and to develop more versatile platforms, large interest has recently arisen in using stimuli−responsive materials as dynamic supports to investigate cell response.[20,58]

Here light−switchable azopolymers are used to imprint several micro−topography optically. Owing to their intrinsic properties, azopolymers may be used as dynamic supports, writing and erasing topographic patterns on purpose.

Following the outline of the thesis is reported with a brief description of each chapter.

The first part of the thesis presents an introduction on the importance of cell−material interaction in tissue engineering, focusing on cell−topography crosstalk and mechanics. Furthermore, azopolymers are presented with a description of their properties and features. Studies on the use of azobenzene−based substrates for cell cultures is very limited and the possibility to exploit their reversibility in biological applications has not been addressed yet. This aspect has been investigated in this thesis. In **Chapter 2** patterned azopolymer films are used as cell culture supports. In more details an holographic set−up is employed to encode diverse patterns, cell behavior is investigated in terms of adhesion and morphology. Reversibility of the imprinted structures is tested by using temperature or light as triggers.

In a first approach cell behavior is investigated a posteriori, that means after pattern manipulation. Thereafter, by using an incoherent and unpolarized light, implemented in a confocal microscopy, it is possible to apply an in situ topographic change. A montage of images shows cell viability after real−time pattern modification. In **Chapter 3** topographic patterns on azopolymers prove to influence cell mechanical properties, besides adhesion and orientation. In fact, cells are stiffer on patterned than on flat surfaces. A study on cell nuclei morphology and cytoskeleton assembly is reported in order to correlate cell elastic properties with cell shape and organization. In **Chapter 4** a new technique to realize precise and complex patterns on azopolymers is presented, based on the use of confocal microscopy. These topographic patterns are suitable for replica−molding technique. Remarkably, this approach proved to be powerful in pattern manipulation in situ, while cells are seeded on the substrates. In fact, owing to the properties of the microscope, that means a thermo−chamber to control biological conditions and a highly spatial resolution given by the laser system, this approach may pave the way to biological study based on dynamic and controlled topographic patterns. Finally, in **Conclusion and Future Prospects** a summary about the main results achieved in this thesis is presented. This study give rise to the introduction of a new class of cell−instructive biomaterials in tissue engineering, synthetic materials upon which topographic signals can be presented on−demand hence investigating and unraveling many processes involved in cell−topography interaction.

1.5 References

(1) Cohen, S.; Baño, M. C.; Cima, L. G.; Allcock, H. R.; Vacanti, J. P.; Vacanti, C. A.; Langer, R. Design of synthetic polymeric structures for cell transplantation and tissue engineering. *Clin. Mater.* **1993**, *13*, 3−10.

(2) Griffith, L. G.; Naughton, G. Tissue engineering−current challenges and expanding opportunities. *Science* **2002**, *295*, 1009−1014.

(3) Bonassar, L. J.; Vacanti, C. A. Tissue engineering: the first decade and beyond. *J. Cell. Biochem.* **1998**, *72*, 297−303.

(4) Lysaght, M. J.; Reyes, J. The growth of tissue engineering. *Tissue Eng.* **2001**, *7*, 485−493.

(5) Ventre, M.; Causa, F.; Netti, P. A. Determinants of Cell–Material Crosstalk at the Interface: Towards engineering of cell instructive materials. *J. Roy. Soc. Interface* **2012**, *9*, 2017−2032.

(6) Ladoux, B.; Nicolas, A. Physically based principles of cell adhesion mechanosensitivity in tissues. *Rep. Prog. Phys.* **2012**, *75*, 116601.

(7) Fletcher, D. A.; Mullins, R. D. Cell mechanics and the cytoskeleton. *Nature* **2010**, *463*, 485−492.

(8) Nobes, C. D.; Hall, A. Rho, rac, and cdc42 GTPases regulate the assembly of multimolecular focal complexes associated with actin stress fibers, lamellipodia, and filopodia. *Cell* **1995**, *81*, 53−62.

(9) Bershadsky, A. D.; Balaban, N. Q.; Geiger, B. Adhesion−dependent cell mechanosensitivity. *Annu. Rev. Cell Dev. Biol.* **2003**, *19*, 677−695.

(10) Singhvi, R.; Stephanopoulos, G.; Wang, D. I. Effects of substratum morphology on cell physiology. *Biotechnol. Bioeng.* **1994**, *43*, 764−771.

(11) Whitesides, G. M.; Ostuni, E.; Takayama, S.; Jiang, X.; Ingber, D. E. Soft lithography in biology and biochemistry. *Annu. Rev. Biomed. Eng.* **2001**, *3*, 335−373.

(12) Xia, Y.; Whitesides, G. M. Soft lithography. *Annu. Rev. Mater. Sci.* **1998**, *28*, 153−184.

(13) Pease, R. Electron beam lithography. *Contemp. Phys.* **1981**, *22*, 265−290.

(14) Hirai, Y.; Yoshida, S.; Takagi, N.; Tanaka, Y.; Yabe, H.; Sasaki, K.; Sumitani, H.; Yamamoto, K. High aspect pattern fabrication by nano imprint lithography using fine diamond mold. *Jpn. J. Appl. Phys.* **2003**, *42*, 3863.

(15) Walboomers, X.; Croes, H.; Ginsel, L.; Jansen, J. Growth Behavior of Fibroblasts on Microgrooved Polystyrene. *Biomaterials* **1998**, *19*, 1861−1868.

(16) Bettinger, C. J.; Langer, R.; Borenstein, J. T. Engineering substrate topography at the micro-and nanoscale to control cell function. *Angew. Chem., Int. Ed.* **2009**, *48*, 5406−5415.
(17) Flemming, R.; Murphy, C.; Abrams, G.; Goodman, S.; Nealey, P. Effects of Synthetic Micro−and Nano−Structured Surfaces on Cell Behavior. *Biomaterials* **1999**, *20*, 573−588.
(18) Discher, D. E.; Janmey, P.; Wang, Y.−l. Tissue cells feel and respond to the stiffness of their substrate. *Science* **2005**, *310*, 1139−1143.
(19) Yim, E. K.; Reano, R. M.; Pang, S. W.; Yee, A. F.; Chen, C. S.; Leong, K. W. Nanopattern−induced changes in morphology and motility of smooth muscle cells. *Biomaterials* **2005**, *26*, 5405−5413.
(20) Davis, K. A.; Burke, K. A.; Mather, P. T.; Henderson, J. H. Dynamic Cell Behavior on Shape Memory Polymer Substrates. *Biomaterials* **2011**, *32*, 2285−2293.
(21) Lekka, M.; Laidler, P.; Gil, D.; Lekki, J.; Stachura, Z.; Hrynkiewicz, A. Elasticity of normal and cancerous human bladder cells studied by scanning force microscopy. *Eur. Biophys. J.* **1999**, *28*, 312−316.
(22) Prabhune, M.; Belge, G.; Dotzauer, A.; Bullerdiek, J.; Radmacher, M. Comparison of mechanical properties of normal and malignant thyroid cells. *Micron* **2012**, *43*, 1267−1272.
(23) Cross, S. E.; Jin, Y.−S.; Rao, J.; Gimzewski, J. K. Nanomechanical analysis of cells from cancer patients. *Nat. Nanotechnol.* **2007**, *2*, 780−783.
(24) González−Cruz, R. D.; Fonseca, V. C.; Darling, E. M. Cellular mechanical properties reflect the differentiation potential of adipose−derived mesenchymal stem cells. *Proc. Natl. Acad. Sci.* **2012**, *109*, E1523−E1529.
(25) McPhee, G.; Dalby, M. J.; Riehle, M.; Yin, H. Can common adhesion molecules and microtopography affect cellular elasticity? A combined atomic force microscopy and optical study. *Med. Biol. Eng. Comput.* **2010**, *48*, 1043−1053.
(26) Khani, M.−M.; Tafazzoli−Shadpour, M.; Rostami, M.; Peirovi, H.; Janmaleki, M. Evaluation of mechanical properties of human mesenchymal stem cells during differentiation to smooth muscle cells. *Ann. Biomed. Eng.* **2013**, 1−8.
(27) Hochmuth, R. M. Micropipette aspiration of living cells. *J. Biomech.* **2000**, *33*, 15−22.
(28) Zhang, H.; Liu, K.−K. Optical tweezers for single cells. *J. Roy. Soc. Interface* **2008**, *5*, 671−690.
(29) Laurent, V. R. M.; Hénon, S.; Planus, E.; Fodil, R.; Balland, M.; Isabey, D.; Gallet, F. O. Assessment of mechanical properties of adherent

living cells by bead micromanipulation: comparison of magnetic twisting cytometry vs optical tweezers. *J. Biomech. Eng.* **2002**, *124*, 408−421.
(30) Radmacher, M. Measuring the elastic properties of biological samples with the AFM. *Eng. in Med. Biol. Magazine, IEEE* **1997**, *16*, 47−57.
(31) Binnig, G.; Quate, C. F.; Gerber, C. Atomic force microscope. *Phys. Rev. Lett.* **1986**, *56*, 930.
(32) Drake, B.; Prater, C.; Weisenhorn, A.; Gould, S.; Albrecht, T.; Quate, C.; Cannell, D.; Hansma, H.; Hansma, P. Imaging crystals, polymers, and processes in water with the atomic force microscope. *Science* **1989**, *243*, 1586−1589.
(33) Radmacher, M.; Tillamnn, R.; Fritz, M.; Gaub, H. From molecules to cells: imaging soft samples with the atomic force microscope. *Science* **1992**, *257*, 1900−1905.
(34) Henderson, E.; Haydon, P.; Sakaguchi, D. Actin filament dynamics in living glial cells imaged by atomic force microscopy. *Science* **1992**, *257*, 1944−1946.
(35) Thomas, G.; Burnham, N. A.; Camesano, T. A.; Wen, Q. Measuring the mechanical properties of living cells using atomic force microscopy. *J. Visualized Exp.* **2013**, e50497−e50497.
(36) Sunyer, R.; Jin, A. J.; Nossal, R.; Sackett, D. L. Fabrication of hydrogels with steep stiffness gradients for studying cell mechanical response. *PloS One* **2012**, *7*, e46107.
(37) Thomas, G.; Burnham, N. A.; Camesano, T. A.; Wen, Q. Measuring the mechanical properties of living cells using atomic force microscopy. *J. Visualized Exp.* **2013**, e50497−e50497.
(38) Zollinger, H. Azo and diazo Chemistry. *Interscience* **1961**.
(39) Rau, H. Photochemistry and photophysics. *CRC Press* **1991**, *2*, pp. 119–141.
(40) Lednev, I. K.; Ye, T.−Q.; Hester, R. E.; Moore, J. N. Femtosecond time−resolved UV−visible absorption spectroscopy of trans−azobenzene in solution. *J. Phys. Chem.* **1996**, *100*, 13338−13341.
(41) Yager, K. G.; Barrett, C. J. Light−induced nanostructure formation using azobenzene polymers. *Polym. Nanostruct. Their Appl. 0* **2006**, 1−38.
(42) Hugel, T.; Holland, N. B.; Cattani, A.; Moroder, L.; Seitz, M.; Gaub, H. E. Single−molecule optomechanical cycle. *Science* **2002**, *296*, 1103−1106.
(43) Han, M.; Ichimura, K. Tilt orientation of p−methoxyazobenzene side chains in liquid crystalline polymer films by irradiation with nonpolarized light. *Macromolecules* **2001**, *34*, 82−89.

(44) Rochon, P.; Batalla, E.; Natansohn, A. Optically induced surface gratings on azoaromatic polymer films. *Appl. Phys. Lett.* **1995**, *66*, 136−138.
(45) Kim, D.; Tripathy, S.; Li, L.; Kumar, J. Laser-induced holographic surface relief gratings on nonlinear optical polymer films. *Appl. Phys. Lett.* **1995**, *66*, 1166−1168.
(46) Marder, S. R.; Kippelen, B.; Jen, A. K.−Y.; Peyghambarian, N. Design and synthesis of chromophores and polymers for electro−optic and photorefractive applications. *Nature* **1997**, *388*, 845−851.
(47) Priimagi, A.; Shevchenko, A. Azopolymer-based micro-and nanopatterning for photonic applications. *J. Polym. Sci. Pol. Phys.* **2014**, *52*, 163−182.
(48) Natansohn, A.; Rochon, P. Photoinduced motions in azo−containing polymers. *Chem. Rev.* **2002**, *102*, 4139−4176.
(49) Priimagi, A.; Kaivola, M.; Virkki, M.; Rodriguez, F. J.; Kauranen, M. Suppression of chromophore aggregation in amorphous polymeric materials: towards more efficient photoresponsive behavior. *J. Nonlinear Opt. Phys. Mater.* **2010**, *19*, 57−73.
(50) Yager, K. G.; Barrett, C. J. Temperature modeling of laser−irradiated azo−polymer thin films. *J. Chem. Phys.* **2004**, *120*, 1089−1096.
(51) Barrett, C. J.; Natansohn, A. L.; Rochon, P. L. Mechanism of optically inscribed high−efficiency diffraction gratings in azo polymer films. *J. Phys. Chem.* **1996**, *100*, 8836−8842.
(52) Pedersen, T. G.; Johansen, P. M.; Holme, N. C. R.; Ramanujam, P.; Hvilsted, S. Mean−field theory of photoinduced formation of surface reliefs in side−chain azobenzene polymers. *Phys. Rev. Lett.* **1998**, *80*, 89.
(53) Kumar, J.; Li, L.; Jiang, X. L.; Kim, D.−Y.; Lee, T. S.; Tripathy, S. Gradient force: the mechanism for surface relief grating formation in azobenzene functionalized polymers. *Appl. Phys. Lett.* **1998**, *72*, 2096−2098.
(54) Bian, S.; Liu, W.; Williams, J.; Samuelson, L.; Kumar, J.; Tripathy, S. Photoinduced surface relief grating on amorphous poly (4−phenylazophenol) films. *Chem. Mater.* **2000**, *12*, 1585−1590.
(55) Baac, H.; Lee, J.−H.; Seo, J.−M.; Park, T. H.; Chung, H.; Lee, S.−D.; Kim, S. J. Submicron−scale topographical control of cell growth using holographic surface relief grating. *Mat. Sci. Eng. C* **2004**, *24*, 209−212.
(56) Rocha, L.; Păiuş, C.−M.; Luca−Raicu, A.; Resmerita, E.; Rusu, A.; Moleavin, I.−A.; Hamel, M.; Branza−Nichita, N.; Hurduc, N. Azobenzene based polymers as photoactive supports and micellar structures for applications in biology. *J. Photoch. Photobio. A* **2014**, *291*, 16−25.

(57) Barillé, R.; Janik, R.; Kucharski, S.; Eyer, J.; Letournel, F. Photo−responsive polymer with erasable and reconfigurable micro− and nano−patterns: an in vitro study for neuron guidance. *Colloids Surf., B* **2011**, *88*, 63−71.
(58) Le, D. M.; Kulangara, K.; Adler, A. F.; Leong, K. W.; Ashby, V. S. Dynamic topographical control of mesenchymal stem cells by culture on responsive poly (ϵ-caprolactone) surfaces. *Adv. Mater.* **2011**, *23*, 3278−3283.

Chapter 2

Reversible Holographic Patterns on Azopolymers for Guiding Cell Adhesion and Orientation

Abstract. Cell−topography interaction has proved to be a powerful tool in guiding cell fate and controlling important biological processes. Micro− and nano−patterned polymers have been largely employed in order to investigate cell mechanotransduction and contact guidance phenomena. Nevertheless among all the available materials, many of them did not allow changes in topography, once the desired shape was imprinted. This chapter is based on a study of NIH−3T3 cells response to reversible topographic signals. Switchable patterns were realized on light responsive azopolymer films by using a conventional holographic set−up. Surface relief gratings (SRGs) were produced with Lloyd's mirror system and erased with circular polarized or incoherent light. Firstly, cell cytoskeleton organization and focal adhesions morphology were studied. Thereafter, pattern reversibility was tested in air and wet environment by using temperature or light as triggers.

Part of the work described in this Chapter has been submitted for publication: Rianna, C.; Calabuig, A.; Ventre, M.; Cavalli, S.; Pagliarulo, V.; Grilli, S.; Ferraro, P.; Netti, P. A. "Reversible holographic patterns on azopolymers for guiding cell adhesion and orientation".

2.1 Introduction

Understanding cellular reaction and response to the external environment is a central aspect in diverse biomedical, bioengineering and clinical applications. A growing number of works is emphasizing the high sensitivity that cells display towards the chemical and physical features of the substrate to which they are connected. In particular, such features proved to affect different aspects of the cell behavior like attachment, spreading, differentiation and ultimately cell fate.[1–6] Different types of signals displayed by the material substrate, such as biochemical, mechanical and topographical signals can influence cell behavior.[7–10] In particular, topographic cues are known to exert a potent influence on cell fate and functions and many techniques were developed to fabricate micro− and nano−grooved materials in order to study contact guidance and mechanotransduction phenomena. The realization of substrates with topographic patterns usually relies on micro− and nano−fabrication techniques, chiefly soft lithography, electron beam or focused ion beam lithography. These techniques, despite possessing a very high spatial resolution, require expensive equipments and are time consuming, especially when large surfaces need to be processed. Additionally, once produced, the geometric features of the master or substrate cannot be readily modified a posteriori since the displayed topography is intrinsically static in nature. In order to overcome the limits of a physically static system and to develop more versatile platforms, large interest has recently arisen in using stimuli−responsive materials as dynamic supports to investigate cell response.[11,12] Along this line, holographic imprinting of surface relief gratings (SRGs) on azopolymer films is a

promising approach for a straightforward fabrication of dynamic substrates. In fact, holographic patterns of linearly polarized light allow the realization of precise and spatially controlled gratings, while circularly polarized or incoherent light enables pattern erasure.[13] Large−scale surface mass displacement was observed by Rochon et al.[14] and by Kim et al.[15] who irradiated azopolymer films with an interference pattern of light. Once the sinusoidal pattern of light is in contact with the polymer, it is able to induce the formation of SRGs, in the form of topographic arrays that trace out the light intensity profile. This phenomenon has been used to realize micro− and nano−grooved polymer films, suitable in many applications, such as optics and photonics.[16,17] Owing to their versatility and intrinsic properties, azo−based materials may have a great impact in unraveling the dynamics of cell adhesion events or in inducing specific adhesion related signaling. Indeed, few examples of SRG applications to cell cultures have been reported.[18−20] However, studies related on dynamic pattern writing/erasing with living cells are lacking. Based on our previous experience on cell response to static micro− and nano−scale patterns,[21−23] we explored the possibility of using light sensitive substrates in order to move toward the development of surfaces on which patterned signals can be manipulated dynamically. Therefore, we investigated the behavior of NIH−3T3 cells on a light sensitive azobenzene−based polymer. Surface production proved to be easy and fast and micron scale patterns were produced with conventional optical equipments. Polymer stability, reversibility and dynamic writing/erasing were investigated. Elongation, orientation and focal adhesion morphology of NIH−3T3 fibroblasts were studied on

different light induced micron−scale topographic patterns. Our data demonstrate that the process we propose is adequate for the production of material platforms to perform in vitro studies on reversible and adjustable topographic patterns. This can in principle allow to investigate cell−topography interactions and mechanotransduction in a dynamic environment.

2.2 Materials and Methods

Poly−Disperse Red 1−methacrylate (pDR1m), Triton X−100, TRITC−phalloidin and HEPES solution were supplied by Sigma. Circular cover glasses were purchased from Thermo Scientific. Chloroform and other solvents were purchased from Romil. Anti−vinculin monoclonal antibody was supplied by Chemicon (EMD Millipore), whereas Alexa Fluor 488 conjugated goat anti−mouse antibody and ToPro3 were purchased from Molecular Probes, Life Technologies.

Circular cover glasses (12 mm diameter) were washed in acetone, sonicated for 15 min and then dried on a hot plate prior to the spin coating process. pDR1m was dissolved in chloroform at a 5% w/v concentration. The solution was spun over the cover glass by using a Laurell spin coater (Laurell Technologies Co.) at 1500 rpm. A Veeco Dektak 150 profilometer was used to monitor the polymer film thickness. Irregular coatings were discarded.

2.2.1 SRG Realization and Erasure

Experiments of SRG realization and erasure with laser light were performed at the CNR−Istituto di Cibernetica "E. Caianiello" in Pozzuoli (Naples), under the supervision of Prof. Pietro Ferraro.

A 442 nm He−Cd laser (power of about 60 mW) was used in a Lloyd's mirror configuration in order to project an interference pattern of light on the azopolymer films, thus inducing mass migration and SRG formation. In more details, the azopolymer sample was glued to one of the mirror's edge and the horizontally polarized laser beam was reflected on it, thus realizing an interference pattern of light. The pattern pitch was given by $2d=\lambda \cdot \sin(\vartheta)$, where λ is the laser wavelength and ϑ is the angle between the incident beam and the mirror. Varying the angle ϑ, patterns with different pitch could be easily prepared. Additionally, a beam from a He−Ne laser emitting at 632 nm was used for a real−time control of the inscription process by monitoring the diffraction efficiency of the inscribed grating. SRG structures can be erased by subjecting them to either high temperatures or light.[24] Temperature induced erasure was performed by means of a hot−plate that was used to heat patterned pDR1m films up to 130 °C, a temperature that is well above the glass transition temperature of the polymer (T_g ~ 85 °C). In the case of light induced erasure, two different strategies were pursued. First, a wave plate−retarder (WPR) was placed between the linear polarized beam (442 nm He−Cd laser) and the sample and acted as polarization filter, thus converting the linear polarized laser beam in a circular polarized one. Time exposure was 10 min. When performing pattern erasure in a wet environment, the circular polarized laser beam was reflected with a mirror on the top

of a fluid filled 35 mm diameter petri−dish. Three different fluid types were tested, namely water, phosphate buffered saline 10x (PBS) and Dulbecco's Modified Eagle Medium (DMEM). Total fluid volume was 1.5 ml and time exposure was 10 min. Second, incoherent light was employed to randomize the azomolecules and erase the SRG inscription. In details, patterned samples were positioned in a petri−dish filled with aqueous solutions and irradiated from the bottom part by using a mercury lamp (15 mW intensity) with a 488 nm filter of a TCS SP5 confocal microscope (Leica Microsystems). Time exposure was 2 min. Substrates were mainly characterized by AFM. In particular, a JPK NanoWizard II (JPK Instruments), mounted on the stage of an Axio Observer Z1 microscope (Zeiss), was used to characterize the azopolymer films in terms of surface topography and pattern features (depth and pitch). Silicon Nitride tips (MSCT, Bruker) with a spring constant of 0.01 N/m were used in contact mode, in air at room temperature. The open source software Fiji[25] was used to measure both pattern height and pattern pitch with the 2D Fast Fourier Transform function.

2.2.2 Cell Culture and Immunofluorescence

NIH−3T3 fibroblasts were cultured in low glucose DMEM and incubated at 37°C in a humidified atmosphere of 95% air and 5% CO_2. Prior to cell seeding, pDR1m substrates were sterilized under UV light for 30 min. In principle, the UV irradiation does not interfere with pDR1m conformation, since the maximum absorption band of the azobenzene polymer is 483 nm (Figure 2.1).

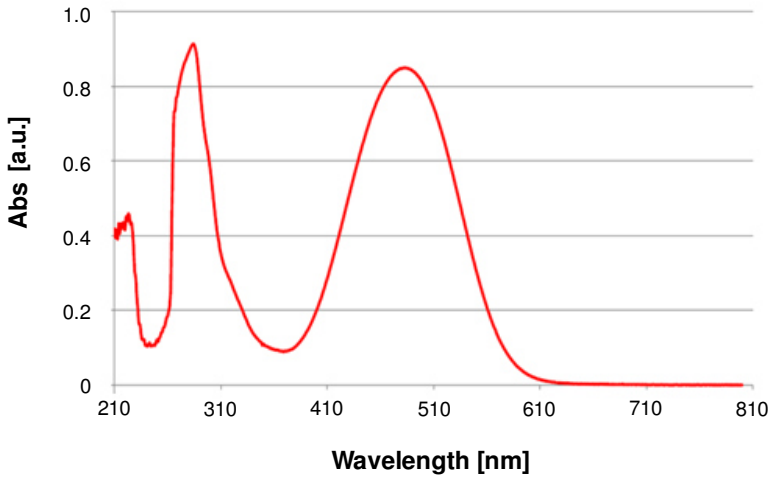

Figure 2.1. UV−Vis absorption spectrum of pDR1m. Maximum absorption wavelength at 483 nm. Analysis was performed by using Cary 100 UV−Vis spectrometer.

After 24 h cells were fixed with 4% paraformaldehyde for 20 min and then permeabilized with 0.1% Triton X−100 in PBS for 3 min. Actin filaments were stained with TRITC−phalloidin. Samples were incubated for 30 min at room temperature in the phalloidin solution (dilution 1:200). Focal adhesions (FAs) were stained with vinculin. Briefly, cells were incubated in an anti−vinculin monoclonal antibody solution (dilution 1:200) for 2 h and then marked with Alexa Fluor 488 conjugated goat anti−mouse antibody (dilution 1:1000) for 30 min at 20°C. Finally, cells were incubated for 15 min at 37°C in ToPro3 solution (dilution 5:1000) to stain cells nuclei. A TCS SP5 confocal microscope (Leica Microsystems) was used to collect fluorescent images of cells on flat and patterned pDR1m films. The laser lines used were 488 nm (vinculin), 543 nm (actin) and 633 nm (nuclei).

Emissions were collected in the 500−530 nm, 560−610 nm and 650−750 nm ranges, respectively. Cell and FA morphometry measurements were performed by using Fiji software. The procedure has been previously described by Ventre et al.[23]

Briefly, cell elongation was assessed from phalloidin stained cells that were analyzed with the MomentMacroJ v. 1.3 script (hopkinsmedicine.org/fae/mmacro.htm). We evaluated the principal moments of inertia (i.e. maximum and minimum) and we defined a cell elongation index as the ratio of the principal moments (Imax/Imin). Cell orientation was defined as the angle that the principal axis of inertia formed with a reference axis, i.e. the pattern direction in the case of SRGs or the horizontal axis for flat surfaces. Morphometric analysis of FAs was performed as follows. Digital images of FAs were first processed using a 15 pixel wide Gaussian blur filter. Then, blurred images were subtracted from the original images using the image calculator command. The images were further processed with the threshold command to obtain binarized images. Pixel noise was erased using the erode command and then particle analysis was performed in order to extract the morphometric descriptors. Only FAs whose length was above 1 μm were included in the statistical analysis.

2.3 Results and Discussion

Azobenzene based polymers undergo to conformational changes when irradiated by light. More specifically, under irradiation with a proper wavelength, the continuous *trans−cis−trans* photo−isomerization of azobenzene molecules, together with their change in geometrical

disposition and polarity, results in a locally preferred orientation of the azobenzene groups, which direct perpendicular to the incident electrical field. As a result, polymer mass migration occurs, thus inducing a pattern inscription on the material surface. Many models have been proposed so far, aiming at elucidating the mechanism of light induced mass transport and consequent pattern formation. Among these, thermal model,[26] pressure gradient force model,[27] mean−field model,[28] optical−field gradient force model[29,30] and athermal photofluidisation[31] have been developed and presented in the last decades. However, a general consensus on the physics that governs SRG formation has not been achieved yet. In this work we used SRGs as cell culture substrates. Topographic patterns were inscribed and erased on pDR1m films by using an interference pattern of light and circularly polarized or incoherent beam respectively. Owing to the photo−reversibility of the azopolymer surface structures, a study of NIH−3T3 cell response to the dynamic topographic changes of SRGs was performed. Lloyd's mirror is a well consolidated set−up that we employed to realize gratings on 700 nm thick pDR1m layers (Figure 2.2A). In details, a linear polarized light reflecting on a mirror resulted in a holographic pattern of light, which was able to inscribe a parallel grating on the interfering azopolymer film surface (Figure 2.2B). By performing a second inscription after rotating the sample by 90°, a two−dimensional (2D) SRG was realized (Figure 2.2C).

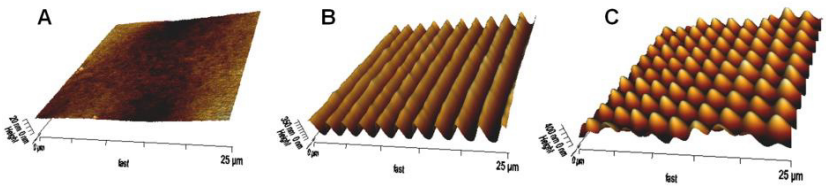

Figure 2.2. 3D AFM images of (A) flat spin coated pDR1m, (B) 2.5 μm pitch pattern realized with an interference pattern of light and (C) 2D grating obtained by two−step illumination, the second grating was inscribed after rotating the sample by 90°.

Patterns with different pitch were prepared by varying the angle between the laser beam and the mirror. Our study was based on linear patterns with nominal pitch of 2.5 and 5.5 μm and two−dimensional grid of 2.5 × 2.5 μm pitch. Table 2.1 shows the measured geometrical features of the patterns, in terms of depth and pitch.

Substrate	Depth [nm]	Pitch [μm]
2.5 μm pattern	332.9 ± 42.9	2.75 ± 0.06
5.5 μm pattern	337.9 ± 25.3	5.60 ± 0.25
2.5×2.5 grid	367.9 ± 101.2	2.55 ± 0.14 (vert) 2.74 ± 0.17 (horiz)

Table 2.1. Dimensions of the geometrical features of the SRGs.

The pattern pitch is in good agreement with the theoretical predefined values. The pitch mismatch observed on the micro grid is probably due to the not perfect overlapping between the two linear patterns. In the following, substrates will be referred to as 2.5 and 5.5 μm linear patterns and 2.5×2.5 μm grid pattern. In order to use these materials as cell culture substrates, we performed a preliminary test to assess pattern stability in conditions comparable to those experienced during cell culture. To this aim, a 2.5 μm linear pattern was scanned with the AFM, thus obtaining the time−zero height profile. Then the sample

was immersed in DMEM at 37°C for 24 h. Afterwards the sample was washed, air dried and scanned with the AFM. Gross morphology of the pattern remained unchanged, as well as the height profile (Figure 2.3), thus demonstrating the structural stability of the substrate in biological conditions.

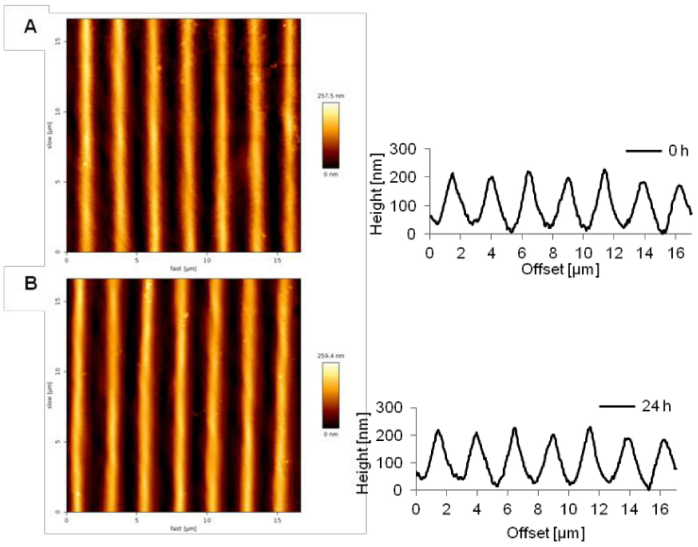

Figure 2.3. AFM height images of (A) 2.5 µm patterned pDR1m film, realized in 10 min of illumination with an interference pattern of light (442 nm laser light, 58 mW) and (B) same sample after 24 hours in DMEM at 37°C. On the right, AFM cross section profiles at time zero and 24 hr.

2.3.1 Cell adhesion, orientation and elongation

NIH−3T3 fibroblast response to the patterned substrates was studied in terms of cell adhesion (FAs length and orientation) and cell shape (elongation and orientation). Flat polymer films were used as control surfaces. Different topographic patterns on azopolymer films proved to exert a strong influence on cell behavior. In fact, NIH−3T3 cells were

mostly round or elliptical in shape when cultivated on either flat or 2.5×2.5 μm grid pattern (Figure 2.4A and 2.4B), whereas they appeared polarized and elongated along the direction of the 2.5 μm (Figure 2.4C) and 5.5 μm linear patterns (Figure 2.4D).

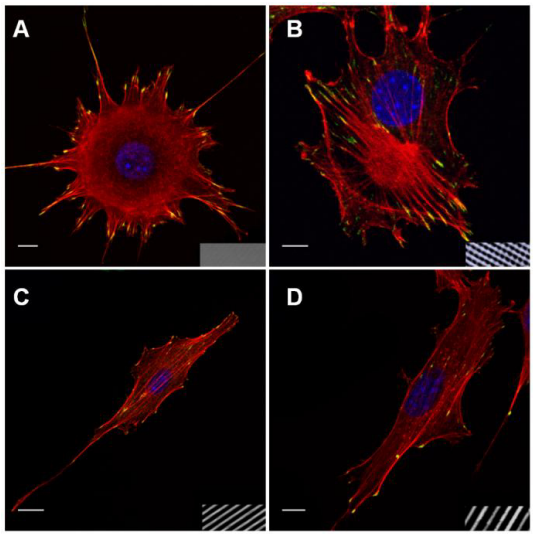

Figure 2.4. Confocal images of NIH−3T3 cells on (A) flat pDR1m, (B) 2.5×2.5 μm grid pattern, (C) 2.5 μm and (D) 5.5 μm linear patterns on pDR1m. Cell cytoskeleton is stained with phalloidin (red), FAs are immunostained for vinculin (green), nuclei are stained with ToPro3 (blue). Transmission images of underlying substrate are shown in the bottom right corner of each confocal micrograph. Scale bars are 10 μm.

Same behavior was observed in case of high cell density, in fact cells were randomly oriented on flat sample (Figure 2.5A) and elongated in the direction of the grating on 2.5 μm linear pattern (Figure 2.5B).

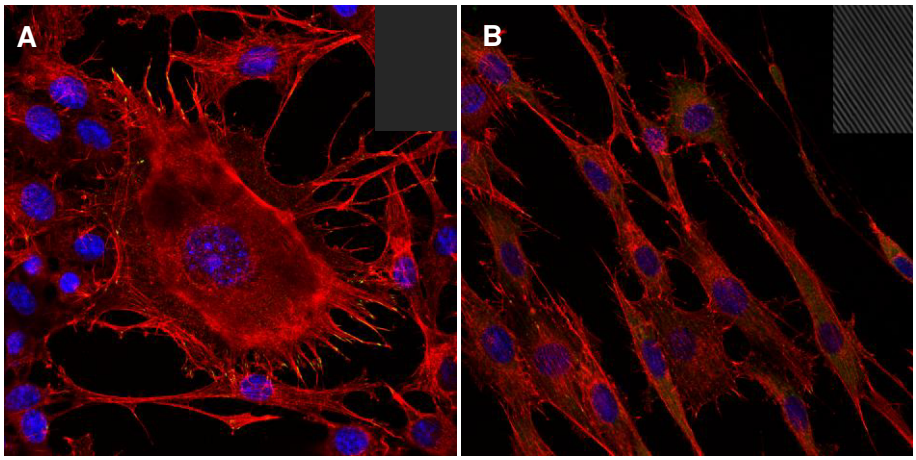

Figure 2.5. Confocal images of high NIH−3T3 cell density on (A) flat pDR1m, (B) 2.5 μm linear patterns on pDR1m. Cell cytoskeleton is stained with phalloidin (red), FAs are immunostained for vinculin (green), nuclei are stained with ToPro3 (blue).

This was confirmed by the quantitative image analysis performed on the confocal micrographs. In more details, the cell elongation (Imax/Imin) was 17.8 ± 2.5 for cells spread on 2.5 μm pattern and 9.5 ± 2.3 on 5.5 μm linear pattern, which were significantly different from those measured on the 2.5×2.5 μm grid and flat pDR1m, i.e 1.5 ± 0.1 and 1.8 ± 0.2, respectively. Regarding orientation, cells were aligned in the same direction of the underlying patterns on 2.5 and 5.5 μm linear gratings, while they were randomly oriented on 2.5×2.5 μm grid and flat polymer (Figure 2.6A). Our results are consistent with other reports that emphasize the role of FA assembly and orientation on cell shape and elongation.[22,23,32] We therefore analyzed the morphological features of FAs on the different topographies and on the flat substrate. FAs that formed on the linear patterns had a comparable length that

was not significantly different from the one measured on the flat substrate. Furthermore, FAs on linear patterns displayed a narrow distribution of orientation angles, whose average values indicated a strong coalignment with the pattern direction. As expected, FAs on flat substrates and on the 2.5×2.5 μm grid were randomly oriented, i.e. mean orientation ~ 45°, with a broad distribution. In particular, FAs on the 2.5×2.5 μm grid, were significantly shorter with respect to those on flat surfaces (Figure 2.6B). Therefore, it is likely that the presence of arrays of dome−shaped pillars hampers the formation of longer focal adhesions.

Thick actin bundles were clearly visible in cells cultured on linear SRG, whereas a predominant cortical actin was observed in cells on flat surfaces. Interestingly, cytoskeletal assemblies that formed in cells on the micro grid had a peculiar rosette−shaped structure. Even though confocal snapshots do not provide information on the dynamics of cytoskeleton assembly, it is tempting to speculate that as micro grids hamper FA formation, the subsequent organization of a stable cytoskeleton is also delayed. Stable actin bundels can only form on a limited number of adhesion spots. The remaining actin is involved in an extensive ruffling at the cell periphery, as the cell tries to maximize the number of adhesions. Indeed, it is recognized that an increased ruffling activity occurs on scarcely adhesive substrates or when the available extracellular adhesive islets are very narrow.[33]

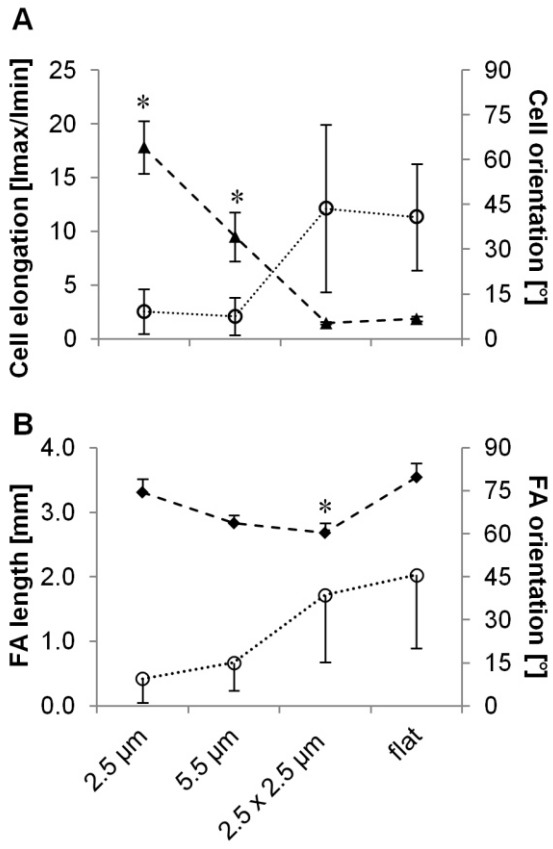

Figure 2.6. (A) Quantitative analysis of the cell elongation index and cell orientation on 2.5 and 5.5 µm linear pattern, 2.5×2.5 µm grid and flat pDR1m. Solid triangles refer to the elongation index, whereas open circles refer to the orientation. (B) Quantitative analysis of the FA length and orientation on the substrates as in (A). Solid diamonds represent FA length, whereas open circles represent FA orientation with respect to the pattern direction. For the grid and flat surface, angles are evaluated with respect to the horizontal axis. Asterisk indicates significant differences with respect to the flat case ($p < 0.05$). Bars refer to standard error of the mean for cell elongation and FA length, whereas they represent the standard deviation in the case of cell and FA orientation.

2.3.2 SRG Reversibility Tests

Topographic patterns imprinted on pDR1m proved to be effective in controlling different aspects of the cell−material interactions and macroscopic cell behavior. More interestingly, though, surface modifications induced on azopolymers are, in principle, reversible, i.e. if exposed to specific chemical/physical cues, patterns can be manipulated or erased. Pattern erasure is an aspect that we carefully addressed as it would greatly increase the versatility of the pDR1m substrates. This could allow to fabricate various patterns on the same substrate without employing expensive equipments or time consuming processes. In this work, pattern erasure was induced by using temperature or light as triggers. In the first case, heating the linear SRG up to 130°C for 3 h caused the flattening of the gratings and the pattern could be rewritten afterwards (Figure 2.7).

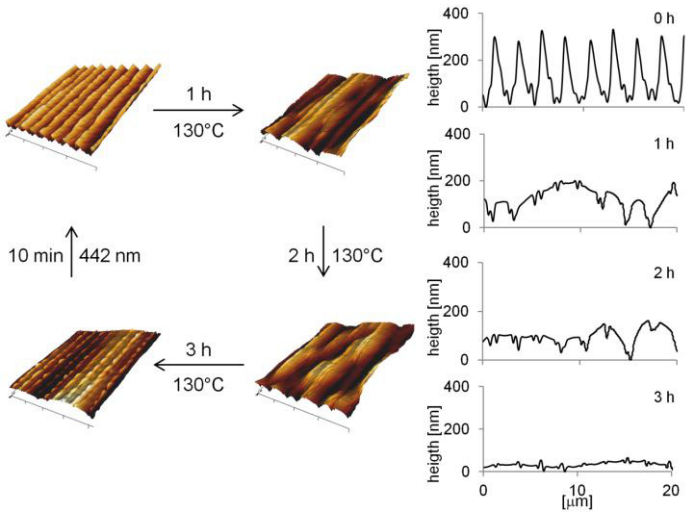

Figure 2.7. 3D AFM images of temperature induced SRG erasure. Temperature was set at 130 °C for 3 h; every hour a 20 × 20 µm AFM image was acquired. A SRG pattern was rewritten on the flat substrate with the

Lloyd's mirror set−up. On the right, height AFM cross sections are shown at different time steps.

Alternatively, circularly polarized light was used to reduce SRG depth. After 10 min of irradiation in air at room temperature, the grating depth decreased from 90 to 10 nm. To assess the effectiveness of pattern modification on cell culture experiment, we first cultivated NIH−3T3 cells on flat surfaces for 24 h. Cells were then trypsinized and the substrates were washed in PBS and air dried. Second, a 2.5 μm pattern was inscribed using the set−up previously described on which cells were seeded on the patterned substrate and cultivated for 24 h. Finally, cells were trypsinized, the substrate was washed and dried and the pattern was erased by exposing it to a circularly polarized light for 10 min at room temperature. In order to draw out quantitative data on cell morphology and adhesion, we prepared a second set of samples in which cells were fixed and stained rather than detached from each substrate with trypsin. Therefore, confocal images of cells stained for vinculin, actin and nuclei were acquired (Figure 2.8). Cells were randomly distributed on flat polymer, while they acquired an elongated morphology when seeded on the linear pattern. Circular polarized light dramatically reduced pattern height and cells recovered a round morphology accordingly. The quantification of cell elongation and orientation is reported in Figure 2.8D, in which the highest values of elongation are measured on the 2.5 μm pattern, whereas the elongation of cells on the erased pattern is not significantly different from the flat case. Accordingly, cell orientation was nearly parallel to the pattern direction with a narrow distribution when cells were seeded on the

pattern, while a random orientation with a broad distribution was measured for cells on both flat and erased pattern. FA length did not display changes in the writing/erasing cycles, whereas FA orientation was very sensitive to the topography as parallel FAs were observed on the SRG only (Figure 2.8E). Therefore, pDR1m coated substrates can in principle be rewritten with different patterns and cells accommodated their behavior accordingly.

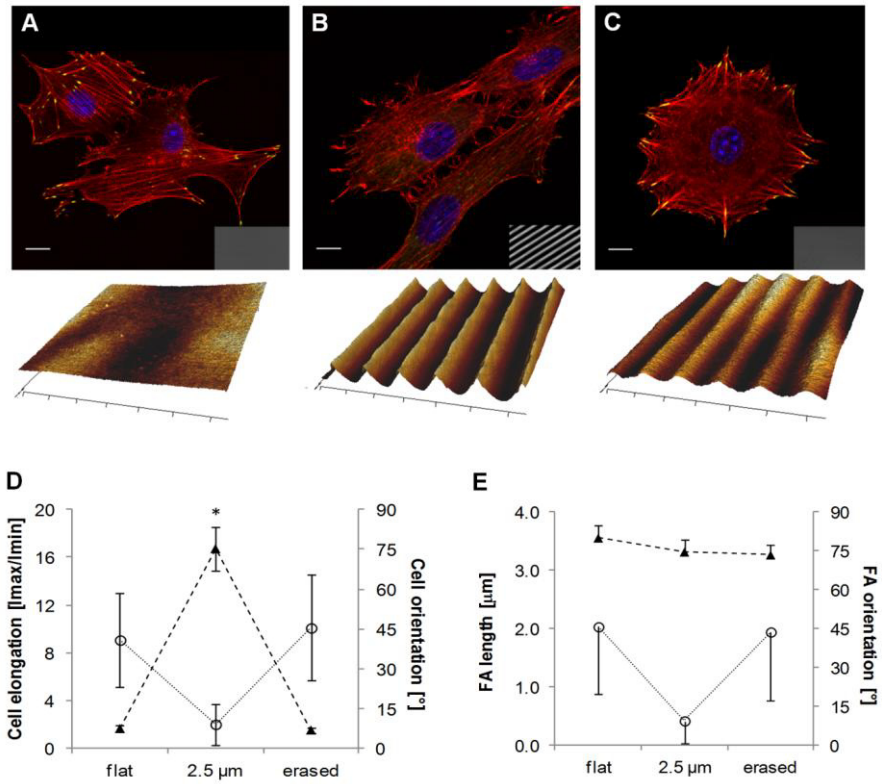

Figure 2.8. Confocal images of NIH−3T3 cultivated on (A) flat pDR1m substrate, (B) SRG grating and (C) pattern erased with circularly polarized light. Transmission images of the substrate are reported in the bottom right corner of each confocal micrograph and AFM scans are shown below them. (D) Plots of the cell elongation (solid triangles) and cell orientation (open circles). (E) Plot of FA length (solid triangles) and orientation (open circles).

Asterisk denotes significant difference with respect to the flat case. Bars indicates standard error of the mean in the case of cell elongation and FA length, whereas they represent standard deviation in the case of cell and FA orientation.

Cells are necessarily cultivated in aqueous media. In order to implement light induced pattern modification or erasure while living cells are cultivated on the substrate, the circularly polarized laser beam must pass through the culturing medium before colliding onto the patterned surface. We then investigated whether the process of pattern erasure was affected by the presence of an aqueous environment. Therefore, the laser beam was directed into the petri−dish containing the SRG sample immersed either in water, PBS or DMEM (1.5 ml in volume). After 10 min of exposure we observed the formation of bubbles−like structures on the polymer surface, which were arranged in a sort of aligned pattern. Simultaneously, the original topographic pattern intensity was drastically reduced. This particular effect occurred independently from the fluid type (Figure 2.9).

As shown in Figure 2.10, cell seeded on the erased SRG were not able to perceive the original topographic signals (red arrow), but rather coaligned along the bubble−like structures (yellow arrow).

The use of circularly polarized light in order to erase or reduce the pattern depth entailed a great disadvantage, in fact optical set−up was hardly adaptable to cell environment conditions and laser intensity was not suitable to dynamic real−time experiments with cells.

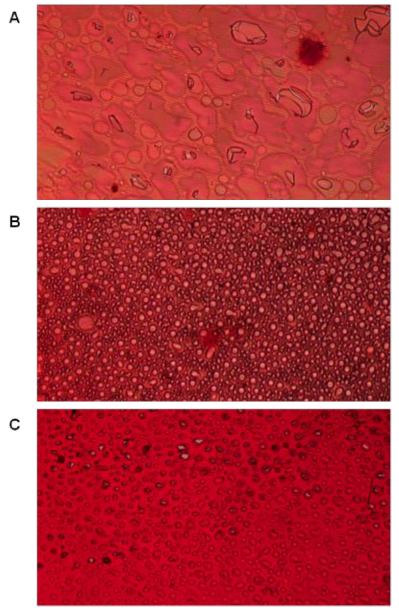

Figure 2.9. Transmission microscope images of patterned pDR1m films after circularly polarized light irradiation in (A) H_2O, (B) PBS and (C) DMEM. Laser intensity was 10 mW and time exposure was 10 min.

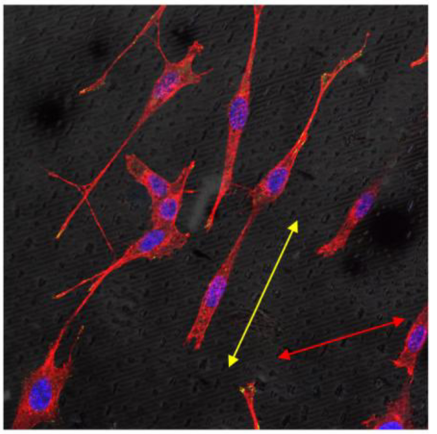

Figure 2.10. Confocal image of NIH−3T3 cells cultivated on a SRG pattern exposed to circularly polarized light in DMEM. Red arrow shows the original pattern direction, whereas the yellow arrow indicates the pattern of the newly formed bubble−like structure, induced by circularly polarized light.

For this reason, we introduced a new approach to erase SRG structures on pDR1m films, based on the use of a microscope. This new strategy was more adaptable to biological conditions, in fact thanks to the microscope equipment it was possible to identify precisely the polymer surface and due to the coupled isolated thermo−chamber, the biological environment was easily reproduced allowing the observation of cells over several hours after light exposure. In this case, an incoherent and unpolarized light beam of a mercury lamp, implemented in a Leica confocal microscope (15 mW intensity, 488 nm filter), was used to erase the patterns. As a matter of fact, incoherent and unpolarized light is highly effective in randomizing azobenzene molecule orientation, as well as circularly polarized one.[34] Starting from these observations, we irradiated a cell populated 2.5 μm pattern for 2 min with the mercury lamp. Also in this case bubble−like structures appeared. However, NIH−3T3 cells were still vital and migrated over the substrate (Figure 2.11A−C).

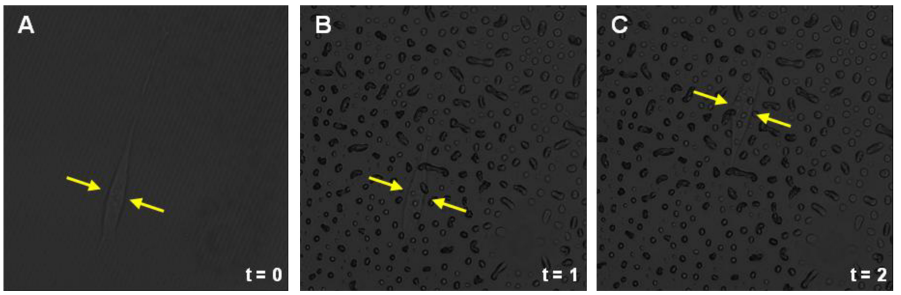

Figure 2.11. Live pattern erasure with mercury lamp. Montage of confocal images of (A) a single cell migrating along the 2.5 μm pattern (t=0), (B) the same location acquired after the 2 min exposure of the incoherent light (t=1) and (C) after 45 min (t=2). Here t stands for three different time snap−shots of a unique time−lapse video. Yellow arrows indicate the cell body at the nuclear position.

Despite both circularly polarized and incoherent light sources proved to be very effective in erasing the pattern in dry condition, the presence of an aqueous environment generates the bubble−like structures either due to scattering of the light or promoting uncontrolled interactions between water and the azopolymer. It is most likely that upon irradiation water molecules deform the polymer, while pDR1m is stable in aqueous media at the normal cell culturing conditions. Therefore, we hypothesize that a photofluidization process (athermal anisotropic photosoftening) occurs, meaning that light induced molecule mobility allows small forces to generate material flow.[35] In an aqueous environment this phenomenon triggers a sort of interfacial phase separation between the hydrophobic polymer and the aqueous environment, with the formation of globular polymeric domains on the substrates. However, this needs to be confirmed with specific experiments.

Azobenzene compounds, along with their response to light irradiation have been widely investigated and are mainly used in the optics and photonics fields. Despite their extraordinary chemical/physical characteristics the number of studies on the use of azobenzene−based substrates for cell cultures is very limited. For instance, Rocha et al.[19] studied the biocompatibility of azopolymers based polysiloxane coatings and investigated the stability of the substrates in aqueous environment. Barille et al.[18] examined the imprinting capabilities of the azo−based photo−switchable materials both in dry and in wet conditions and analyzed neuron response to the topographic signal. Interestingly, they also reported that irregularities were observed when the pattern was embossed in the presence of PBS. To the best of our

knowledge, however, the possibility to exploit writing/erasing reversibility of azobenzene polymers in biological applications has not been addressed yet. We demonstrated that pDR1m coated glass can be patterned in a reversible manner using either temperature or light triggers. Additionally, the microscopy set−up we propose allows the pattern feature alteration in presence of cells without affecting their viability. However, even though the system has the potential to be employed for real−time experiments with living cells, the irradiation technique need to be optimized in order to gain a better control on the azopolymer mass transport and hence improving pattern modification.

2.4 Conclusions

In this chapter an effective technique to imprint and modify biocompatible topographic patterns on azopolymer pDR1m coated glass, using conventional optical equipments (i.e. Lloyd's mirror set-up), is presented. Patterned substrates proved to be effective in confining FA growth and cytoskeletal assembly. Pattern could be easily erased and rewritten in dry conditions, whereas in a wet environment circularly polarized or incoherent light were able to alter pattern shape. In particular, microscopy set-up with incoherent and unpolarized light−mediated erasure proved to be a promising strategy for real−time experiments with living cells as exposure time did not affect cell viability. Therefore, the system we proposed has the potential to be employed for understanding cell behavior and possibly mechanotransduction events in a dynamic environment.

2.5 References

(1) Walboomers, X.; Croes, H.; Ginsel, L.; Jansen, J. Growth behavior of fibroblasts on microgrooved polystyrene. *Biomaterials* **1998**, *19*, 1861−1868.
(2) McNamara, L. E.; McMurray, R. J.; Biggs, M. J.; Kantawong, F.; Oreffo, R. O.; Dalby, M. J. Nanotopographical control of stem cell differentiation. *J. Tissue Eng.* **2010**, *1*, 120623.
(3) Ladoux, B.; Nicolas, A. Physically based principles of cell adhesion mechanosensitivity in tissues. *Rep. Prog. Phys.* **2012**, *75*, 116601.
(4) Biggs, M. J. P.; Richards, R. G.; Dalby, M. J. Nanotopographical modification: a regulator of cellular function through focal adhesions. *Nanomedicine* **2010**, *6*, 619−633.
(5) Yim, E. K.; Darling, E. M.; Kulangara, K.; Guilak, F.; Leong, K. W. Nanotopography−induced changes in focal adhesions, cytoskeletal organization, and mechanical properties of human mesenchymal stem cells. *Biomaterials* **2010**, *31*, 1299−1306.
(6) Ventre, M.; Valle, F.; Bianchi, M.; Biscarini, F.; Netti, P. A. Cell fluidics: producing cellular streams on micropatterned synthetic surfaces. *Langmuir* **2011**, *28*, 714−721.
(7) Hallab, N.; Bundy, K.; O'Connor, K.; Clark, R.; Moses, R. Cell adhesion to biomaterials: correlations between surface charge, surface roughness, adsorbed protein, and cell morphology. *J. Long−Term Eff. Med. Implants* **1994**, *5*, 209−231.
(8) Flemming, R.; Murphy, C.; Abrams, G.; Goodman, S.; Nealey, P. Effects of synthetic micro−and nano−structured surfaces on cell behavior. *Biomaterials* **1999**, *20*, 573−588.
(9) Yeung, T.; Georges, P. C.; Flanagan, L. A.; Marg, B.; Ortiz, M.; Funaki, M.; Zahir, N.; Ming, W.; Weaver, V.; Janmey, P. A. Effects of substrate stiffness on cell morphology, cytoskeletal structure, and adhesion. *Cell Motil. Cytoskeleton* **2005**, *60*, 24−34.
(10) Ventre, M.; Causa, F.; Netti, P. A. Determinants of cell–material crosstalk at the interface: towards engineering of cell instructive materials. *J. R. Soc., Interface* **2012**, *9*, 2017−2032.
(11) Davis, K. A.; Burke, K. A.; Mather, P. T.; Henderson, J. H. Dynamic cell behavior on shape memory polymer substrates. *Biomaterials* **2011**, *32*, 2285−2293.

(12) Le, D. M.; Kulangara, K.; Adler, A. F.; Leong, K. W.; Ashby, V. S. Dynamic topographical control of mesenchymal stem cells by culture on responsive poly (ϵ-caprolactone) surfaces. *Adv. Mater.* **2011**, *23*, 3278−3283.
(13) Natansohn, A.; Rochon, P. Photoinduced motions in azo−containing polymers. *Chem. Rev.* **2002**, *102*, 4139−4176.
(14) Rochon, P.; Batalla, E.; Natansohn, A. Optically induced surface gratings on azoaromatic polymer films. *Appl. Phys. Lett.* **1995**, *66*, 136−138.
(15) Kim, D.; Tripathy, S.; Li, L.; Kumar, J. Laser-induced holographic surface relief gratings on nonlinear optical polymer films. *Appl. Phys. Lett.* **1995**, *66*, 1166−1168.
(16) Marder, S. R.; Kippelen, B.; Jen, A. K.−Y.; Peyghambarian, N. Design and synthesis of chromophores and polymers for electro−optic and photorefractive applications. *Nature* **1997**, *388*, 845−851.
(17) Priimagi, A.; Shevchenko, A. Azopolymer-based micro-and nanopatterning for photonic applications. *J. Polym. Sci., Part B: Polym. Phys.* **2014**, *52*, 163−182.
(18) Barillé, R.; Janik, R.; Kucharski, S.; Eyer, J.; Letournel, F. Photo−responsive polymer with erasable and reconfigurable micro− and nano−patterns: an in vitro study for neuron guidance. *Colloids Surf., B* **2011**, *88*, 63−71.
(19) Rocha, L.; Păiuş, C. M.; Luca−Raicu, A.; Resmerita, E.; Rusu, A.; Moleavin, I. A.; Hamel, M.; Branza Nichita, N.; Hurduc, N. Azobenzene based polymers as photoactive supports and micellar structures for applications in biology. *J. Photochem. Photobiol., A* **2014**, *291*, 16−25.
(20) Baac, H.; Lee, J.−H.; Seo, J.−M.; Park, T. H.; Chung, H.; Lee, S.−D.; Kim, S. J. Submicron−scale topographical control of cell growth using holographic surface relief grating. *Mater. Sci. Eng., C* **2004**, *24*, 209−212.
(21) Iannone, M.; Ventre, M.; Formisano, L.; Casalino, L.; Patriarca, E. J.; Netti, P. A. Nanoengineered surfaces for focal adhesion guidance trigger mesenchymal stem cell self−organization and tenogenesis. *Nano Lett.* ***2015****, 15, 1517−1525.*
(22) Natale, C. F.; Ventre, M.; Netti, P. A. Tuning the material−cytoskeleton crosstalk via nanoconfinement of focal adhesions. *Biomaterials* **2014**, *35*, 2743−2751.
(23) Ventre, M.; Natale, C. F.; Rianna, C.; Netti, P. A. Topographic cell instructive patterns to control cell adhesion, polarization and migration. *J. R. Soc., Interface* **2014**, *11*, 20140687.

(24) Jiang, X.; Li, L.; Kumar, J.; Kim, D.; Tripathy, S. Unusual polarization dependent optical erasure of surface relief gratings on azobenzene polymer films. *Appl. Phys. Lett.* **1998**, *72*, 2502−2504.
(25) Schindelin, J.; Arganda−Carreras, I.; Frise, E.; Kaynig, V.; Longair, M.; Pietzsch, T.; Preibisch, S.; Rueden, C.; Saalfeld, S.; Schmid, B. Fiji: an open−source platform for biological−image analysis. *Nat. methods* **2012**, *9*, 676−682.
(26) Yager, K. G.; Barrett, C. J. Temperature modeling of laser−irradiated azo−polymer thin films. *J. Chem. Phys.* **2004**, *120*, 1089−1096.
(27) Barrett, C. J.; Natansohn, A. L.; Rochon, P. L. Mechanism of optically inscribed high−efficiency diffraction gratings in azo polymer films. *J. Phys. Chem.* **1996**, *100*, 8836−8842.
(28) Pedersen, T. G.; Johansen, P. M.; Holme, N. C. R.; Ramanujam, P.; Hvilsted, S. Mean−Field Theory of photoinduced formation of surface reliefs in side−chain azobenzene polymers. *Phys. Rev. Lett.* **1998**, *80*, 89.
(29) Kumar, J.; Li, L.; Jiang, X. L.; Kim, D.−Y.; Lee, T. S.; Tripathy, S. Gradient force: the mechanism for surface relief grating formation in azobenzene functionalized polymers. *Appl. Phys. Lett.* **1998**, *72*, 2096−2098.
(30) Bian, S.; Liu, W.; Williams, J.; Samuelson, L.; Kumar, J.; Tripathy, S. Photoinduced surface relief grating on amorphous poly (4−phenylazophenol) films. *Chem. Mater.* **2000**, *12*, 1585−1590.
(31) Hurduc, N.; Donose, B. C.; Macovei, A.; Paius, C.; Ibanescu, C.; Scutaru, D.; Hamel, M.; Branza−Nichita, N.; Rocha, L. Direct observation of athermal photofluidisation in azo−polymer films. *Soft matter* **2014**, *10*, 4640−4647.
(32) Biela, S. A.; Su, Y.; Spatz, J. P.; Kemkemer, R. Different sensitivity of human endothelial cells, smooth muscle cells and fibroblasts to topography in the nano–micro range. *Acta Biomater.* **2009**, *5*, 2460−2466.
(33) Lutz, R.; Pataky, K.; Gadhari, N.; Marelli, M.; Brugger, J.; Chiquet, M. Nano−stenciled RGD−gold patterns that inhibit focal contact maturation induce lamellipodia formation in fibroblasts. *PloS One* **2011**, *6*, e25459.
(34) Yager, K. G.; Barrett, C. J. Light−induced nanostructure formation using azobenzene polymers. *Polym. Nanostruct. Their Appl.* **2006**, 1−38.
(35) Karageorgiev, P.; Neher, D.; Schulz, B.; Stiller, B.; Pietsch, U.; Giersig, M.; Brehmer, L. From anisotropic photo−fluidity towards nanomanipulation in the optical near−field. *Nat. Mater.* **2005**, *4*, 699−703.

Chapter 3

Cell Mechanics Investigation on Patterned Azopolymers by Using AFM Technique

Abstract. Physical and chemical characteristics of materials are potent regulators of cell behavior. In particular, cell elasticity is a fundamental parameter that reflects the state of a cell. Surface topography finely regulates cell fate and function via adhesion mediated signalling and cytoskeleton generated forces. However, how topographies alter cell mechanics is still unclear. In this work we have analyzed the mechanical properties of peripheral and nuclear regions of NIH−3T3 cells on polymer substrates with different topographic patterns. Micron scale patterns in the form of parallel ridges or square lattices of surface elevations were encoded on reversible light responsive azopolymer films. The techniques employed for pattern inscription were based on contactless optical methods. Cell mechanics was investigated by atomic force microscopy (AFM). Cells and consequently cell cytoskeleton were oriented along the linear patterns affecting cytoskeletal structures, e.g. formation of actin stress fibres. Cytoskeleton generated forces, modulated by substrate topography, deform the nucleus changing its morphology and its mechanical properties. Our data demonstrate that topographic substrate patterns are recognized by cells and mechanical information is transferred by the cytoskeleton up to the nucleus.

The work described in this Chapter is part of a manuscript in preparation: Rianna, C.; Ventre, M.; Cavalli, S.; Radmacher, M.; Netti, P. A. "Micropatterns regulate cell mechanics through the material−cytoskeleton crosstalk".

3.1 Introduction

Understanding the interactions between cells and the extracellular environment for creating favourable conditions when designing functional biomaterials is one of the critical aspects of tissue engineering.[1,2] Within this context, the presence of adhesive ligands plays a crucial role. In particular, natural extracellular matrix (ECM) regulates via mechanical,[3] biochemical,[4] or topographical cues,[5] many cell processes eventually determining the cellular behavior. Biomaterial surfaces with engineered physical/chemical features have been developed in the last years in order to control and guide cell fate and functions.[6–8] Even though the biochemical mechanisms regulating the transduction of adhesive signals into a biological response are not thoroughly understood, there is growing evidence that focal adhesion (FA) mediated signalling and cytoskeleton−generated forces play a fundamental role.[9] Cell adhesion and cytoskeletal assemblies are the major responsible for the determination of the cell mechanical behavior. Indeed, cell elasticity can be largely influenced by the cell−substrate interface interactions. Moreover, in the last years, cell mechanics investigation has proven to be a promising tool for applications in the field of regenerative medicine, in which cell mechanical properties can be quantitative markers, monitoring the regulation of cell differentiation,[10–12] or within clinical and medical contexts as in cancer diagnostics.[13,14] Cell mechanics can be evaluated with several methods, such as micropipette aspiration,[15] optical tweezers,[16] magnetic twisting cytometry,[17] or atomic force microscopy (AFM).[18] Among these, AFM is the most widely used technique for adherent cells, allowing both topographical imaging and measuring

mechanical properties of heterogeneous living samples, such as cells. Since its invention,[19] the AFM has become an important tool for studying surface and mechanical properties very first of hard samples, but soon its potential for soft and biological samples was discovered.[20–22] By obtaining force−distance AFM curves, cell elastic properties can be measured in terms of elastic or Young's modulus.[18] In order to understand the interaction between ECM signals and cell mechanics, several studies have been performed. For example it has been shown that cell spreading and stiffness directly depend on mechanical properties of the underlying materials.[23,24] Even though topographic cues proved to be a powerful tool to control different aspects of the cell behavior, there are only few reports concerning the effects of topographies on cell mechanics. In particular, submicron scale topographic patterns were reported to alter the FA – cytoskeleton – nuclear shape axis[25] and changes in nuclear morphology might have a direct impact on gene expression.[26] However, the possible interplays between topography and nuclear mechanics have not been clarified yet. Furthermore, topographic signals in vivo might change in time and space owing to active cellular remodelling or to deformation arising from external forces. Therefore, it is of great interest analysing topography mediated mechanotransduction in a dynamic environment. This would require the development of materials able to display topographic signals whose features can be modulated dynamically.

In this study we investigated the influence of microgrooved patterns on the local elasticity of fibroblast cells, their cytoskeletal organization and the shape of cell nuclei. Micropatterns were fabricated using azopolymers and cell mechanics was investigated with AFM.

Topographies were encoded on the material surfaces in a contactless manner by means of either structured light or with a laser beam. AFM measurements were performed locally in order to gain information on cell stiffness in specific cell regions. Our data demonstrated that topography induces specific cytoskeletal structures, which interact with the nucleus affecting its shape and volume. Furthermore, cytoskeleton mediated deformations cause changes in the nuclear mechanical properties.

3.2 Materials and Methods

Cell mechanics study was performed on four kinds of patterns imprinted on pDR1m films. First 2.5 μm periodicity parallel linear grating and 2.5 × 2.5 μm grid pattern were encoded with a Lloyd's mirror set−up (as described in Chapter 2). Moreover, 5 μm periodicity parallel linear pattern was produced on pDR1m with single laser induced patterning technique,[27, 28] which will be described in chapter 4. In the following, substrates will be referred to as 2.5 or 5 μm linear patterns and 2.5 × 2.5 μm grid pattern.

3.2.1 Detecting Cell Mechanical Properties by AFM

Experiments of cell mechanics have been performed at the Institute for Biophysics, University of Bremen, under the supervision of Prof. Manfred Radmacher.

A MFP3D AFM (Asylum Research, Santa Barbara, CA, USA) was used to measure topography and mechanical properties of live cells.

An optical microscope was combined to the AFM to be able to control tips and samples. Soft cantilevers (MLCT, Bruker, nominal spring constant 0.01 N/m) were used to investigate cell properties. Petri dishes were fixed to an aluminum holder with vacuum grease and mounted on the AFM stage with two magnets, all the set−up was enclosed in a homebuilt polymethylmethacrylate (PMMA) box in order to maintain 5% CO_2. For imaging the AFM was operated in contact mode at a scan rate of 1 line per second. During force mapping, spring constant of cantilever was first calibrated by using a thermal tune method.[29] Force curves were typically recorded at a scan rate of 1 Hz, corresponding to a maximum loading rate of 1nN/s and a maximum force of 1nN. Typically, 400 force curves were measured over a cell area of 30 x 30 μm. Mechanical properties of cells, in terms of Young's modulus (E) values were estimated from each force curve within a force map. Evaluation was performed with the date analysis package IGOR (Wavemetrics). The Hertzian model was used to calculate Young's modulus for every force curve, therefore 400 values were generated for each force map. The median was calculated from these values as a representative modulus of each force volume.

3.2.2 Cell Culture and Staining Procedures

NIH−3T3 fibroblasts were cultured on patterned azopolymer films, following the procedure described in Chapter 2 (paragraph 2.2.2). After 48 hours from cell seeding, NIH−3T3 fibroblasts were fixed with 4% paraformaldehyde for 20 min and then permeabilized with 0.1% Triton X−100 in PBS 1x for 3 min. Actin filaments were stained with

TRITC−phalloidin. Samples were incubated for 30 min at room temperature in the phalloidin solution (dilution 1:200). For focal adhesion (FA) staining, cells were immersed in an anti−vinculin monoclonal antibody solution (dilution 1:200) for 2 h and labelled with Alexa Fluor 488 conjugated goat anti−mouse antibody (dilution 1:1000) for 30 min. Finally, cells were incubated for 15 min at 37°C in a To−Pro3 solution (dilution 5:1000) to stain cell nuclei. Leica TCS SP5 confocal microscope (Leica Microsystems) was used to collect fluorescent images of cells, the laser lines used were 488 nm (vinculin), 543 nm (actin) and 633 nm (nuclei). Emissions were collected in the 500−530 nm, 560−610 nm and 650−750 nm ranges, respectively. Fiji software[30] was used to measure cell nuclei aspect ratio and volume from 3D z−stacks.

3.3 Results and Discussion

AFM technique was used to investigate mechanical properties of NIH−3T3 cells subjected to different topographic patterns. Several gratings were realized on spin coated azopolymer pDR1m films by using Lloyd's mirror set−up and single laser induced patterning technique (Figure 3.1). In this chapter the influence of pattern shape and periodicity on cell stiffness was examined. 48 hours prior to AFM data acquisition, cells were seeded on flat pDR1m, 2.5 and 5 μm linear gratings and 2.5 x 2.5 μm grid pattern. Commercial polystyrene (PS) petri−dishes and bare glass slides were used as control surfaces.

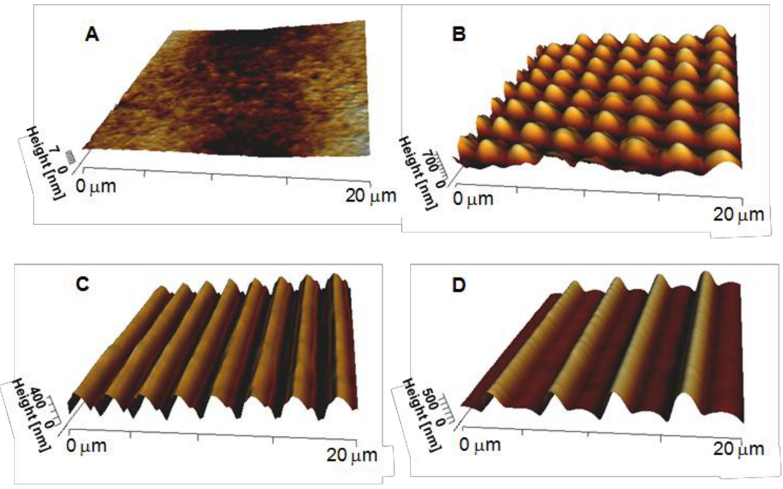

Figure 3.1. Three−dimensional height AFM images of (A) flat spin coated pDR1m on bare glass, (B) 2.5 µm pitch linear pattern on pDR1m realized by using the Lloyd's mirror technique, (C) 2.5 × 2.5 µm grid pattern obtained by overlapping two orthogonal patterns with the Lloyd's mirror technique; (D) 5 µm pitch linear pattern embossed on pDR1m with the single laser beam technique. Image size is 20 × 20 µm.

3.3.1 Analysis of Mechanical Properties on Several Cell Regions

Since cells are not homogenous elastic materials, their mechanical properties are strongly dependent on position. In order to discriminate the diverse mechanical response of the selected cell compartments, we performed force maps on three different regions, namely cell body, nuclear, and peripheral areas (Figure 3.2A). In Figure 3.2B is reported the 3D image of the same cell and Figure 3.2C and 3.2D show logarithmic scale elastic moduli (logE) and cell height map, respectively.

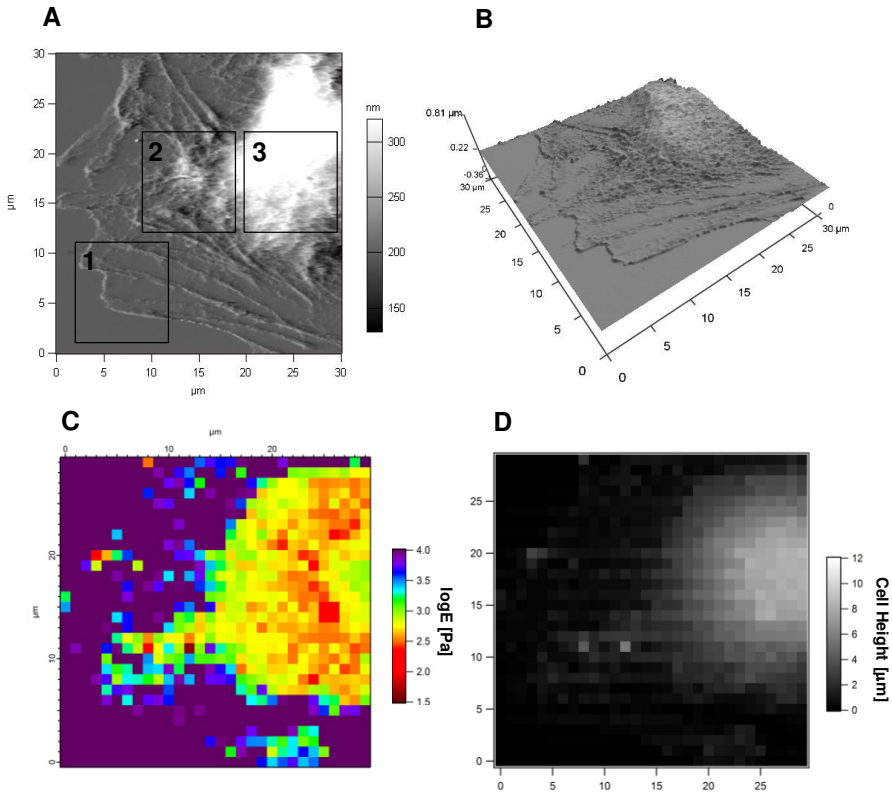

Figure 3.2. (A) Deflection AFM image of a cell spread on bare glass. Three squares are showing the regions over which force maps were scanned, (1) peripheral region, (2) cell body and (3) nuclear region. (B) 3D image of the same cell, (C) logarithmic scale of elastic moduli map and (D) cell height map.

Typically 400 force curves were measured over a cell area of either 10 x 10 µm or 20 x 20 µm. Figure 3.3 shows logarithmic plots of elastic modulus values on nuclear regions, cell body and peripheral regions of NIH−3T3 cells spread on petri−dishes (black color), glass cover slips (light blue), flat pDR1m (green), 5 µm pattern (violet), 2.5 x 2.5 µm grid pattern (red) and 2.5 µm pattern (orange). Results are shown as box plot diagrams in which average values of all elastic moduli from

each force map are represented as cross markers, the box defined the 25th and 75th percentile ranges and the bars are median values.

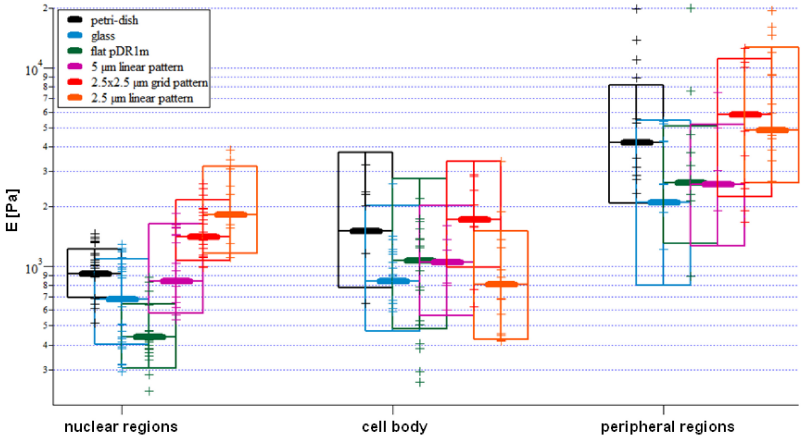

Figure 3.3. Logarithmic plot of elastic modulus values on nuclear regions, cell body and peripheral regions of NIH−3T3 cells spread on petri−dishes (black color), glass cover slip (light blue), flat pDR1m (green), 5 µm pattern (violet), 2.5 x 2.5 µm grid pattern (red) and 2.5 µm pattern (orange). The results are shown as box plot diagrams, in which cross markers represent the average of elastic modulus values from every force maps and thick bar markers represent their median value.

Results showed that elastic properties of cells vary with position, i.e. E moduli were generally lower in the nuclear and higher in the peripheral region. In particular, a strong dependence of cellular elasticity on topography and geometry of the underlying substrates was demonstrated. Force mapping allowed us to calculate the mechanical properties of different cellular regions. In normal conditions, for example cells cultivated on isotropic flat substrates, local elastic moduli can vary up to two orders of magnitude within the same cell, depending on the cell region (Figure 3.4A). Lower moduli were

generally observed in the thicker areas of the cell, e.g. on the cell nuclear region. Conversely, the stiffest cell regions corresponded to thinner cell processes like lamellipodia or lamellae. However, due to the thinness of cells in these areas the apparent Young's modulus observed in AFM is much larger than the true modulus.[31,32] Contrarily, when we performed force mappings on cells cultivated on linear patterns we observed more uniform distributions in terms of elastic moduli and cell heights (Figure 3.4B).

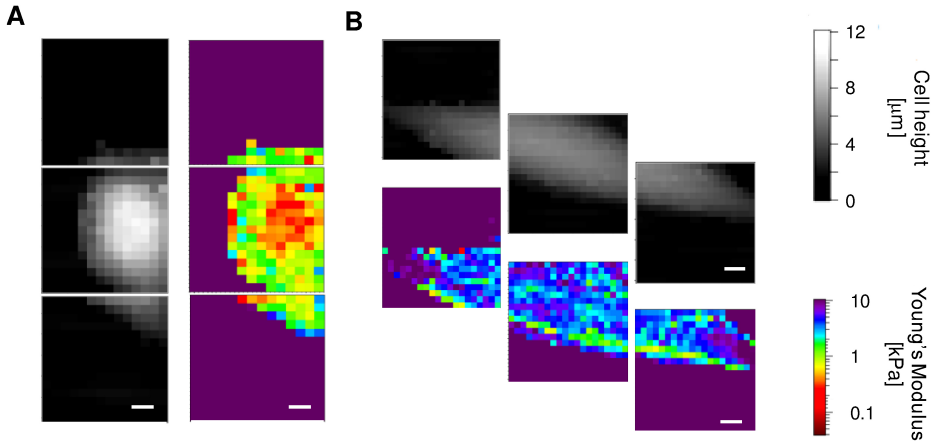

Figure 3.4. Height and elasticity maps of NIH−3T3 cells on (A) flat pDR1m and (B) 2.5 µm pitch linear pattern. Maps are 30 × 30 µm with pixels of 1.5 µm. Greyscale map refers to cell heights, whereas color map refers to Young's modulus values. Scale bars are 5 µm.

3.3.2 Comparing Cell Mechanical Properties to Cell Height

To gain a better insight into the dependence of Young's modulus on cell height, we collected 1500−2000 force curves on cells for each substrate type, from which we extracted the elastic moduli and the

contact point, whence we deduced the local cell height. The data of Young's modulus versus cell height are presented in Figure 3.5.

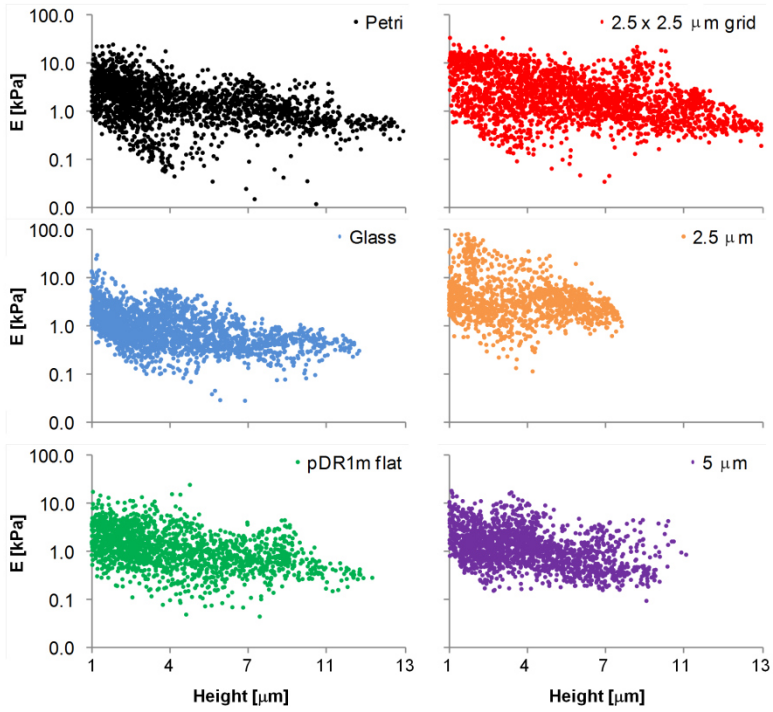

Figure 3.5. Semi−log scatter plots of cell Young's modulus (E) versus cell height for the different substrates.

Generally, we observed a softening of the modulus with increasing cell height. To exclude the influence of the substrate on the apparent elastic modulus, cell heights below 1 µm were excluded from the analysis. Indeed, we measured "non physiological" moduli (approximately 10^5 Pa) corresponding to the thin regions like lamellae and lamellipodia, which is a well known artefact for thin samples.[33] Force and height AFM maps did not allow us to discriminate univocally the diverse cell

regions. An alternative way would have been to label selected cell components, such as the nucleus and the cytoskeleton with fluorescent vital stains. These, even if conventionally classified as vital, need to be translocated into the cytoplasm for example with electroporation or lipofectants. This was reported to affect mechanical properties to a certain extent.[34] To discriminate the mechanical behavior of the different cell regions we followed a more conservative approach. More specifically, we avoided the use of staining and considered the whole distribution cell heights. Moduli corresponding to the top 5% of heights were considered as representative of the mechanical stiffness of the nuclear region. Conversely, we considered as elastic moduli of the cell body those calculated in a range around the median of all cell heights values (corresponding to the range between the 40 and 60% percentile). According to this classification we found that fibroblasts cultivated on patterned substrates possessed a significantly stiffer cell body. More specifically, the highest modulus was recorded on the 2.5 μm linear pattern, which was significantly higher than that measured on the 2.5 × 2.5 μm grid substrates and on the 5 μm patterns (Figure 3.6A). Similar results were observed in the case of nuclear modulus in which stiffer nuclei were found on the 2.5 μm linear pattern, whereas cells on the 2.5 × 2.5 μm grid and on the 5 μm linear pattern had nuclear regions with comparable stiffness (Figure 3.6B).

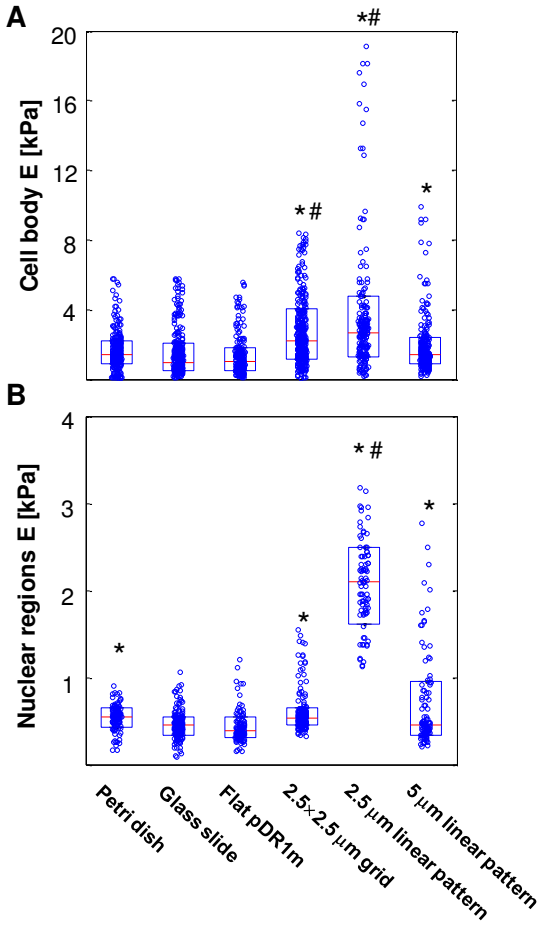

Figure 3.6. Box plots of the Young's modulus of (A) cell body and (B) nuclear regions of cells seeded on the different substrates. Blue boxes enclose the 1st and 3rd quartiles, whereas the red mark is the median value. Blue open circles are the individual measurements. * indicates significant differences with respect to the flat pDR1m substrate ($p < 0.05$); # indicates significant differences with respect to the 5 μm linear pattern ($p < 0.05$).

We then investigated whether a dependency between cell body mechanics and nuclear mechanics existed.

We found a positive dependency between the elastic moduli of the two cell regions, with the only exception of the cells cultivated on the 2.5 × 2.5 μm grid that displayed a relatively high cell body stiffness and an intermediate nuclear one (Figure 3.7).

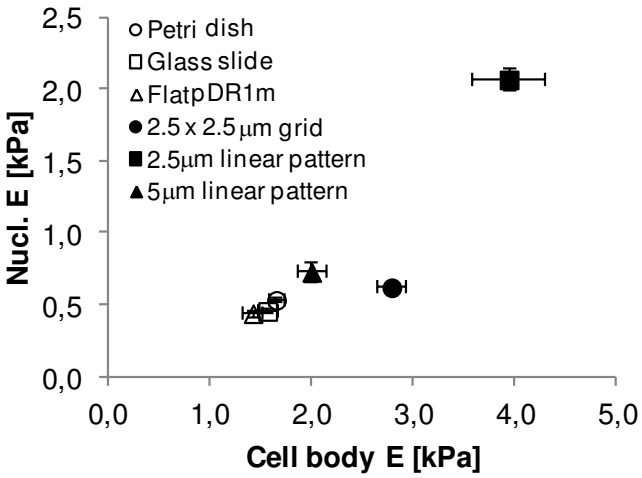

Figure 3.7. Scatter plot of the cell nuclear Young's modulus (Nucl. E) versus cell body Young's modulus (Cell body E). Bars are standard error of the mean.

3.3.3 Cell Nuclei Morphology and Cytoskeleton Organization

The actin cytoskeleton is known to play a central role in determining mechanical properties of cells.[35,36] Additionally, being linked to the nucleus through the LINC complexes, actin bundles can deform the nucleus thus altering its mechanical response.[35] Therefore, we wanted to investigate if surface patterning could affect cytoskeletal assemblies and how these could alter nuclear shape and mechanics.

Cells on 2.5 μm linear pattern were highly elongated and the majority of stress fibres ran along the entire cell body length being oriented along the pattern direction (Figure 3.8A). Actin bundle were frequently seen in close contact with the nucleus and some fibres faithfully traced out nuclear contours, suggesting an active squeezing of the nuclear envelope, which consequently appeared oblong in shape. Cells on the 5 μm linear pattern were less elongated and displayed a number of thick actin bundles remote from the nucleus. In this case, the nucleus was also elliptical in shape, however not as oblong as that seen on the 2.5 μm pattern (Figure 3.8B). A very different cytoskeleton structure has formed in cells on the 2.5 × 2.5 μm grid pattern in which a sparse network of thick and radially assembled fibres was observed (Figure 3.8C). Such a network was always located between the nucleus and the basal cell membrane. Lateral or apical stress fibres around the nucleus were almost absent and, as a consequence, the nucleus appeared spherical in shape. Cells on flat pDR1m substrates displayed a broad spectrum of morphologies ranging from spindle−like to circularly−shaped cells (Figure 3.8D). Similarly, an actin cytoskeleton with aligned bundles was predominantly observed in spindle−like cells whereas a more isotropic network with randomly distributed fibres was seen in circular cells.

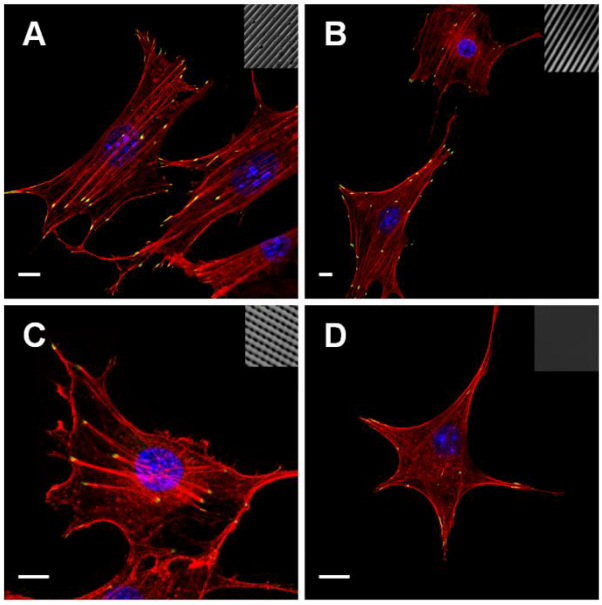

Figure 3.8. Confocal images of NIH−3T3 cell labelled with rhodamine phalloidin (cytoskeleton), vinculin (focal adhesions) and To−Pro 3 (nuclei). Cells were cultivated on (A) 2.5 μm linear pattern; (B) 5 μm linear pattern; (C) 2.5 × 2.5 μm grid and (D) flat pDR1m. Scale bars are 10 μm.

Owing to the diversity of the cytoskeletal assemblies on the substrates and the apparent shape of the nucleus, we asked whether a dependency between nuclear morphology and stiffness existed. Therefore, we evaluated the aspect ratio (A/R) of the nuclear projected area and the nuclear volume and we plotted the Young's modulus against these parameters.

Softer nuclei are characterized by low A/R values, ranging in the 1.2 – 1.5 interval (Figure 3.9A). Even though cells on 5 μm patterns displayed nuclei with an higher A/R value, nuclear stiffness was not significantly different to that measured in the case of cells on Petri dish

and on the 2.5 × 2.5 μm grid. Nuclei of cells cultivated on 2.5 μm linear patterns exhibited the highest value of A/R, although not significantly different from the one of cells on the 5 μm pattern, and the highest elastic modulus. Therefore, the A/R of the projected nuclear area does not correlate well with the mechanical properties. Lateral compressive forces are not very effective in altering nuclear mechanical properties probably because the nucleus can freely expand in the orthogonal direction. This prompted us to investigate the effects of the nuclear volume changes on the mechanical properties. With the exception of cells grown on bare glass slides, we found a much stronger dependence of nuclear stiffness on nuclear volume (Figure 3.9B). Highly elongated cells, as those on the 2.5 μm pattern, possess oblong and smaller nuclei that are also the stiffest ones. Closely packed acting bundles wrapping around the nuclear envelope are likely to exert substantial mechanical stress that ultimately compresses the nucleus. This is reasonable as the nuclear membrane is known to be porous and a volume reduction necessarily leads to a chromatin condensation.[37] This determines an increase of the nuclear modulus. Higher nuclear volumes were observed in the case of cells having the cytoskeleton, at least partly, disengaged from the nucleus, as 2.5 × 2.5 μm grid and flat pDR1m. In these cases, the cytoskeletal structure is not able to exert a coordinated nuclear compression and subsequent volume reduction. Accordingly, nuclear modulus is low. An exception is represented by the nuclei of cells on bare glass. It is therefore possible that surface mechanics or chemistry, besides topography, can affect nuclear mechanics.[31,38] Unfortunately, we were not able to measure nuclear volume of cells cultivated on Petri dishes owing to the

thickness of the polystyrene bottom that provided noisy 3D z−stacks. In particular, FA mediated signalling might alter the level of actomyosin contractility and hence the magnitude of the forces acting on the nuclear envelope.

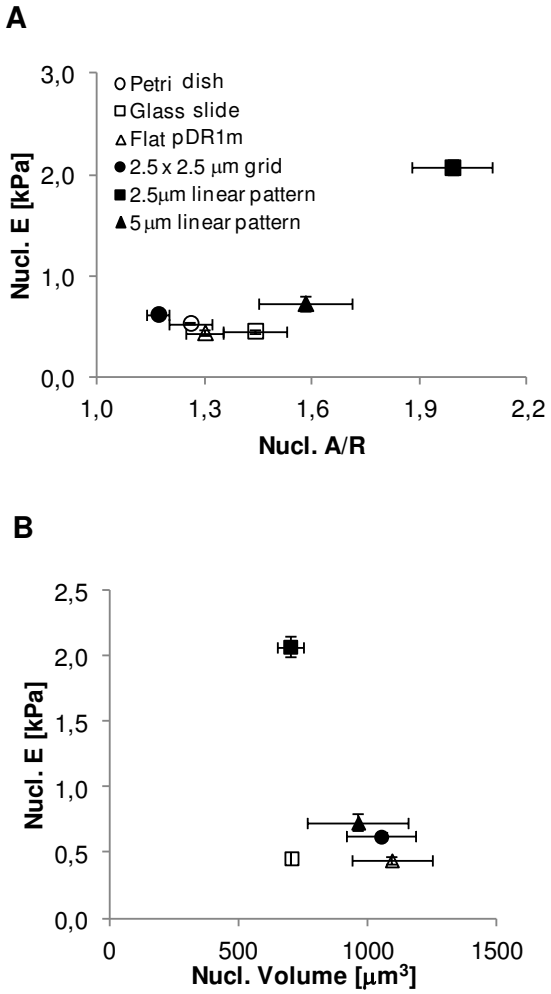

Figure 3.9. Scatter plots of the nuclear Young's modulus (Nucl. E) versus (A) nuclear A/R and (B) nuclear volume. Bars represent standard error of the mean.

Figure 3.10 shows cell nuclei shape on different substrates, oblong on the linear pattern and roundish on the isotropic cell culture supports. Cell nuclei were clearly oriented in the direction of the underlying linear patterns, as confirmed by the plot in Figure 3.11.

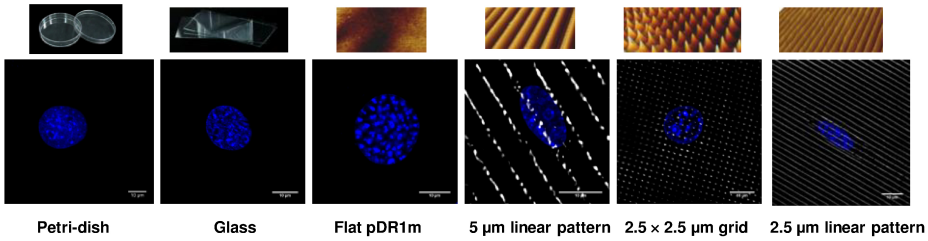

Figure 3.10. Confocal images of cell nuclei on different substrates. Starting from the left to the right, cell nucleus on petri−dish, glass, flat pDR1m, 5 µm linear pattern, 2.5 × 2.5 µm grid and 2.5 µm linear pattern on pDR1m. Scale bars are 10 µm. On the top of confocal micrographs, AFM images show substrate topography.

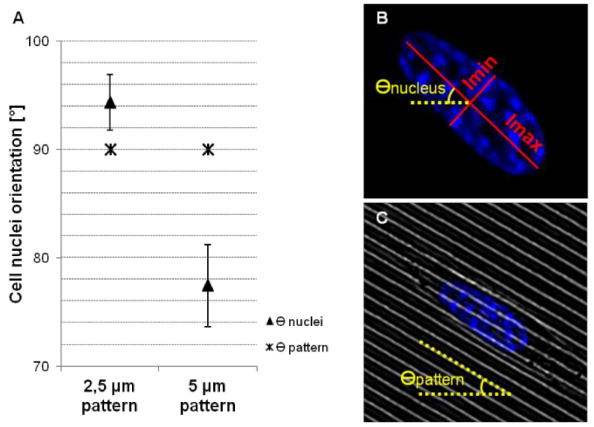

Figure 3.11. (A) Cell nuclei orientation on patterned pDR1m films. Triangle makers refer to the angle Θ formed between the main axis of cell nuclei and the reference axis, star markers represent the angle between the linear patterns and the reference axis. (B) Fluorescent image of cell nuclei, stained with ToPro3, red lines represent main axis of cell nucleus (maximum and minimum). The angle between Imax and the reference axis is shown in

yellow. (C) Transmission image of 2.5 μm linear pattern, dashed yellow lines represent the angle between the parallel linear grating and the reference axis.

Cell mechanics is strongly affected by environmental cues. In particular, the physical/mechanical characteristics of the supporting material are known to exert a potent effect on cell stiffness. Several studies were focused in elucidating the effect of the substrate's properties on cell stiffness using various techniques.[15−18] Generally, more rigid materials provoke cells to become stiffer, whereas soft materials, as hydrogels, make the cells more compliant.[23,24] These findings are of particular interest not only in diagnostics as altered cellular mechanical properties might underlie some kind of pathologies, but also in regenerative medicine since the transduction of exogenous mechanical signals can ultimately dictate cell fate and functions.[6,39,40] Despite such detailed knowledge on materials stiffness and mechanotransduction, the effects of surface topography on cell mechanics have been, in comparison, scarcely investigated. Along these lines, Hansen et al.[38] studied the elasticity of MC3T3−E1 cells on flat and nano−structured polymeric substrates. They found that cells on the nanometer−sized topographical features were stiffer than those cultivated on flat control substrates. Similarly, McPhee et al.[11] reported that NIH−3T3 fibroblasts displayed higher mechanical properties on microgrooved elastomeric substrates with respect to cells cultivated on flat controls. More recently, McKee et al.[41] found that the geometrical features of patterned substrates affect both nuclear shape and modulus. They hypothesized that the nucleus could directly act as a mechanosensor of the substrate topography, whose signals can

influence cell alignment and proliferation. Our results are in general agreement with these reports. However, we not only found that topographic signals alter nuclear shape and mechanics, but we also highlighted how cytoskeletal assemblies and cell body mechanics are regulated by the underlying micropattern. In fact, confocal micrographs revealed diverse cytoskeletal structures that formed on the topographies and these structures interacted differently with the nucleus. Indeed, actin bundles are connected to the nuclear envelope with specific linkers and therefore changes in the cytoskeletal structures can be directly transferred to the nucleus. Additionally, actomyosin generated forces can stand on the nuclear envelope thus altering its structure dynamically. Versaevel et al.[37] found that lateral compressive forces generated by actin bundles regulated nuclear orientation and deformation. Cells cultivated on micropatterned adhesive islands developed anisotropic contraction dipoles that altered nuclear shape and induced chromatin condensation. In our experiments, microtopographies act at the level of FAs by confining their formation and guiding their growth. As we have recently reported,[42] in the case of narrow ridges, as in 2.5 μm patterns, FAs forming orthogonal to the pattern direction are unstable and more prone to collapse upon actin contraction. Such a collapse not only causes the cytoskeleton to be coaligned with the pattern, but also that the cell acquires a narrow spindle−like morphology with a highly elongated nucleus (Figure 3.8A and 3.9A). Furthermore, the coordinated contraction exerted by the actin cytoskeleton all around the nucleus causes a significant volume decrease (Figure 3.9B). Altogether, shape and volume changes can be responsible for nuclear

matter densification and hence an increase of the measured stiffness. Larger features, and more specifically larger ridges as in the 5 μm linear patterns, enable the FAs to grow up to significant lengths even in directions orthogonal to that of the pattern. In this case, cells can acquire a more spread morphology with a cytoskeleton that is distributed all over the cell body (Figure 3.8B). Here, the nucleus is less stressed with respect to what found in the 2.5 μm pattern case, and takes on a less compressed shape (Figure 3.9A and B). Accordingly, nuclear modulus was lower. A very peculiar response of the NIH−3T3 to the 2.5 × 2.5 μm grid was observed. Such a substrate allowed FAs to establish only on a limited area and their maturation was inhibited by the small size of the topographic features. Cells usually displayed ragged edges and the cytoskeleton was constituted by few bundles arranged in star−shaped manner (Figure 3.8C). This structure formed between the pattern and the nucleus. Nuclear envelope was apparently disengaged from the actin cytoskeleton as the nucleus was thicker (Figure 3.5), rounder (Figure 3.9A) and more compliant (Figure 3.6B). Taken together these data demonstrate that topographic patterns are very effective in modulating the material−cytoskeleton crosstalk. Patterns regulate cytoskeleton assembly and hence nuclear shape along with the forces acting on the nuclear envelope. These observations can be in principle used to design topographic patterns able to transfer mechanical information up to the nucleus thus influencing cell fate and functions.

3.4 Conclusions

In this work we showed that micropatterned substrates strongly influence cell mechanical properties of cell body and region around the nucleus. In particular, we found that fibroblasts cultured on 2.5 and 5 μm linear patterns possessed significantly stiffer bodies and nuclei, in comparison to those cultured on flat controls or isotropic grid patterns (2.5 × 2.5 grid). Since the actin cytoskeleton is known to play a critical role in determining cell mechanical properties and is physically connected to cell nuclei, we investigated cytoskeleton assemblies and nuclei morphology to gain a better insight into the material−cytoskeleton crosstalk. Primarily, we found that the elastic properties of the cell body were directly proportional to those of nuclear regions. Moreover, a connection between cell nuclei mechanical proprieties and morphology was found. In fact, in comparison with cell nuclei on flat controls, cell nuclei on linear patterns showed an higher aspect ratio, a lower volume and stiffer values of Young moduli. In other words, highly elongated cells, as those on the 2.5 μm and 5 μm linear pattern, possessed oblong and smaller nuclei that were also the stiffest ones. Closely packed acting bundles wrapping around the nuclear envelope are likely to exert substantial mechanical stress that ultimately compresses the nucleus, increasing its stiffness. Our work proved that topographic signals can be used as critical tools to control and direct mechanical properties of cells. This result may become useful in the development of new cell−instructive biomaterials for tissue engineering.

3.5 References

(1) Lutolf, M.; Hubbell, J. Synthetic biomaterials as instructive extracellular microenvironments for morphogenesis in tissue engineering. *Nat. Biotechnol.* **2005**, *23*, 47−55.
(2) Sengupta, D.; Waldman, S. D.; Li, S. From in vitro to in situ tissue engineering. *Ann. Biomed. Eng.* **2014**, 1−9.
(3) Yeung, T.; Georges, P. C.; Flanagan, L. A.; Marg, B.; Ortiz, M.; Funaki, M.; Zahir, N.; Ming, W.; Weaver, V.; Janmey, P. A. Effects of substrate stiffness on cell morphology, cytoskeletal structure, and adhesion. *Cell Motil. Cytoskeleton* **2005**, *60*, 24−34.
(4) Van Kooten, T. G.; Spijker, H. T.; Busscher, H. J. Plasma−treated polystyrene surfaces: model surfaces for studying cell–biomaterial interactions. *Biomaterials* **2004**, *25*, 1735−1747.
(5) Flemming, R.; Murphy, C.; Abrams, G.; Goodman, S.; Nealey, P. Effects of synthetic micro−and nano−structured surfaces on cell behavior. *Biomaterials* **1999**, *20*, 573−588.
(6) Engler, A. J.; Sen, S.; Sweeney, H. L.; Discher, D. E. Matrix elasticity directs stem cell lineage specification. *Cell* **2006**, *126*, 677−689.
(7) Kilian, K. A.; Bugarija, B.; Lahn, B. T.; Mrksich, M. Geometric cues for directing the differentiation of mesenchymal stem cells. *Proc. Natl. Acad. Sci.* **2010**, *107*, 4872−4877.
(8) Dalby, M. J.; Gadegaard, N.; Tare, R.; Andar, A.; Riehle, M. O.; Herzyk, P.; Wilkinson, C. D.; Oreffo, R. O. The control of human mesenchymal cell differentiation using nanoscale symmetry and disorder. *Nat. Mater.* **2007**, *6*, 997−1003.
(9) McNamara, L. E.; McMurray, R. J.; Biggs, M. J.; Kantawong, F.; Oreffo, R. O.; Dalby, M. J. Nanotopographical control of stem cell differentiation. *J. Tissue Eng.* **2010**, *1*, 120623.
(10) González−Cruz, R. D.; Fonseca, V. C.; Darling, E. M. Cellular mechanical properties reflect the differentiation potential of adipose−derived mesenchymal stem cells. *Proc. Natl. Acad. Sci.* **2012**, *109*, E1523−E1529.
(11) McPhee, G.; Dalby, M. J.; Riehle, M.; Yin, H. Can common adhesion molecules and microtopography affect cellular elasticity? A combined atomic force microscopy and optical study. *Med. Biol. Eng. Comput.* **2010**, *48*, 1043−1053.
(12) Khani, M.−M.; Tafazzoli−Shadpour, M.; Rostami, M.; Peirovi, H.; Janmaleki, M. Evaluation of mechanical properties of human mesenchymal

stem cells during differentiation to smooth muscle cells. *Ann. Biomed. Eng.* **2013**, 1−8.
(13) Lekka, M.; Laidler, P.; Gil, D.; Lekki, J.; Stachura, Z.; Hrynkiewicz, A. Elasticity of normal and cancerous human bladder cells studied by scanning force microscopy. *Eur. Biophys. J.* **1999**, *28*, 312−316.
(14) Prabhune, M.; Belge, G.; Dotzauer, A.; Bullerdiek, J.; Radmacher, M. Comparison of mechanical properties of normal and malignant thyroid cells. *Micron* **2012**, *43*, 1267−1272.
(15) Hochmuth, R. M. Micropipette aspiration of living cells. *J. Biomech.* **2000**, *33*, 15−22.
(16) Zhang, H.; Liu, K.−K. Optical tweezers for single cells. *J. R. Soc., Interface* **2008**, *5*, 671−690.
(17) Laurent, V. r. M.; Hénon, S.; Planus, E.; Fodil, R.; Balland, M.; Isabey, D.; Gallet, F. o. Assessment of mechanical properties of adherent living cells by bead micromanipulation: comparison of magnetic twisting cytometry vs optical tweezers. *J. Biomech. Eng.* **2002**, *124*, 408−421.
(18) Radmacher, M. Measuring the elastic properties of biological samples with the AFM. *Eng. Med. Biol. Magazine, IEEE* **1997**, *16*, 47−57.
(19) Binnig, G.; Quate, C. F.; Gerber, C. Atomic force microscope. *Phys. Rev. Lett.* **1986**, *56*, 930.
(20) Drake, B.; Prater, C.; Weisenhorn, A.; Gould, S.; Albrecht, T.; Quate, C.; Cannell, D.; Hansma, H.; Hansma, P. Imaging crystals, polymers, and processes in water with the atomic force microscope. *Science* **1989**, *243*, 1586−1589.
(21) Radmacher, M.; Tillamnn, R.; Fritz, M.; Gaub, H. From molecules to cells: imaging soft samples with the atomic force microscope. *Science* **1992**, *257*, 1900−1905.
(22) Henderson, E.; Haydon, P.; Sakaguchi, D. Actin filament dynamics in living glial cells imaged by atomic force microscopy. *Science* **1992**, *257*, 1944−1946.
(23) Sunyer, R.; Jin, A. J.; Nossal, R.; Sackett, D. L. Fabrication of hydrogels with steep stiffness gradients for studying cell mechanical response. *PloS One* **2012**, *7*, e46107.
(24) Thomas, G.; Burnham, N. A.; Camesano, T. A.; Wen, Q. Measuring the mechanical properties of living cells using atomic force microscopy. *J. Visualized Exp.* **2013**, e50497−e50497.
(25) Natale, C. F.; Ventre, M.; Netti, P. A. Tuning the Material−cytoskeleton crosstalk via nanoconfinement of focal adhesions. *Biomaterials* **2014**, *35*, 2743−2751.

(26) Ramdas, N. M.; Shivashankar, G. Cytoskeletal control of nuclear morphology and chromatin organization. *J. Mol. Biol.* **2014**.
(27) Bian, S.; Li, L.; Kumar, J.; Kim, D.; Williams, J.; Tripathy, S. Single laser beam−induced surface deformation on azobenzene polymer films. *Appl. Phys. Lett.* **1998**, *73*, 1817−1819.
(28) Ambrosio, A.; Camposeo, A.; Carella, A.; Borbone, F.; Pisignano, D.; Roviello, A.; Maddalena, P. Realization of submicrometer structures by a confocal system on azopolymer films containing photoluminescent chromophores. *J. Appl. Phys.* **2010**, *107*, 083110.
(29) Hutter, J. L.; Bechhoefer, J. Calibration of atomic-force microscope tips. *Rev. Sci. Instrum.* **1993**, *64*, 1868−1873.
(30) Schindelin, J.; Arganda−Carreras, I.; Frise, E.; Kaynig, V.; Longair, M.; Pietzsch, T.; Preibisch, S.; Rueden, C.; Saalfeld, S.; Schmid, B. Fiji: an open−source platform for biological−image analysis. *Nat. Methods* **2012**, *9*, 676−682.
(31) Domke, J.; Dannöhl, S.; Parak, W. J.; Müller, O.; Aicher, W. K.; Radmacher, M. Substrate dependent differences in morphology and elasticity of living osteoblasts investigated by atomic force microscopy. *Colloids Surf., B* **2000**, *19*, 367−379.
(32) Gavara, N.; Chadwick, R. S. Determination of the elastic moduli of thin samples and adherent cells using conical atomic force microscope tips. *Nat. Nanotechnol.* **2012**, *7*, 733−736.
(33) Rotsch, C.; Jacobson, K.; Condeelis, J.; Radmacher, M. EGF−stimulated lamellipod extension in adenocarcinoma cells. *Ultramicroscopy* **2001**, *86*, 97−106.
(34) Fuhrmann, A.; Staunton, J.; Nandakumar, V.; Banyai, N.; Davies, P.; Ros, R. AFM stiffness nanotomography of normal, metaplastic and dysplastic human esophageal cells. *Phys.Biol.* **2011**, *8*, 015007.
(35) Moeendarbary, E.; Valon, L.; Fritzsche, M.; Harris, A. R.; Moulding, D. A.; Thrasher, A. J.; Stride, E.; Mahadevan, L.; Charras, G. T. The cytoplasm of living cells behaves as a poroelastic material. *Nat. Mater.* **2013**, *12*, 253−261.
(36) Rotsch, C.; Radmacher, M. Drug−induced changes of cytoskeletal structure and mechanics in fibroblasts: an atomic force microscopy study. *Biophys. J.* **2000**, *78*, 520−535.
(37) Versaevel, M.; Grevesse, T.; Gabriele, S. Spatial coordination between cell and nuclear shape within micropatterned endothelial cells. *Nat. Commun.* **2012**, *3*, 671.

(38) Hansen, J. C.; Yul Lim, J.; Xu, L.−C.; Siedlecki, C. A.; Mauger, D. T.; Donahue, H. J. Effect of surface nanoscale topography on elastic modulus of individual osteoblastic cells as determined by atomic force microscopy. *J. Biomech.* **2007**, *40*, 2865−2871.
(39) Denais, C.; Lammerding, J., Nuclear mechanics in cancer. In *Cancer Biology and the Nuclear Envelope*, Springer: 2014; pp 435−470.
(40) Swift, J.; Ivanovska, I. L.; Buxboim, A.; Harada, T.; Dingal, P. D. P.; Pinter, J.; Pajerowski, J. D.; Spinler, K. R.; Shin, J.−W.; Tewari, M. Nuclear lamin−A scales with tissue stiffness and enhances matrix−directed differentiation. *Science* **2013**, *341*, 1240104.
(41) McKee, C. T.; Raghunathan, V. K.; Nealey, P. F.; Russell, P.; Murphy, C. J. Topographic modulation of the orientation and shape of cell nuclei and their influence on the measured elastic modulus of epithelial cells. *Biophys. J.* **2011**, *101*, 2139−2146.
(42) Ventre, M.; Natale, C. F.; Rianna, C.; Netti, P. A. Topographic cell instructive patterns to control cell adhesion, polarization and migration. *J. Roy. Soc. Interface* **2014**, *11*, 20140687.

Chapter 4

Pattern Inscription on Azopolymers by Confocal Microscopy Technique: an in Vitro Approach For Dynamic Cell Guidance

Abstract. Here we report a simple and fast technique to produce submicrometric patterns on azopolymers by using a well known and largely used instrument in the biologic field: the confocal microscope. Owing to the properties of azopolymers, the polarized confocal laser light allows a surface mass migration and the formation of defined structures in a selected area. Thanks to the stability of the imprinted shapes, patterned azopolymers can be used as versatile molds in replica−molding technique or for cell culture study. Remarkably, with this technique it is possible to realize patterns meanwhile cells are seeded on the substrate and to perform a real−time investigation on their response accordingly to the new topography. This study may pave the way to a new class of cell−instructive biomaterials: synthetic materials upon which topographic signals can be presented on−demand, hence investigating and unraveling complex processes in cell−topography interaction. In fact, this interaction has proved to be a key factor when designing a new material for tissue engineering.

The work presented in this chapter is part of a manuscript in preparation: Rianna, C.; Kollarigowda, R.; Ventre, M.; Cavalli, S.; Netti, P. A. "Pattern realization on azopolymers by using confocal microscope: a fast technique for replica−molding and cell culture applications".

4.1 Introduction

Azopolymers are unique and attractive materials in which the azobenzene molecules photo−isomerization can lead to a macroscopic material motion, also named light−induced molecular displacement or mass migration.[1, 2] In fact, if illuminated with a polarized light with a proper wavelength, the azobenzene molecules undergo to a reversible *trans−cis−trans* isomerization process, moving and changing their orientation perpendicularly to the polarization direction of the irradiating light.[3, 4] During last decades, several phenomena arising from azopolymers−light interaction have been observed and described. Among these, surface relief gating (SRG) formation has gained large attention due to the possibility of generating periodic patterns thanks to structured light (as described in Chapter 2). [5−11] Despite their enormous potentialities and applicability, the realization of SRGs requires an optical set−up, made of powerful lasers, tools and filters able to induce a holographic pattern of polarized light. This involves dedicated equipments and hardware, but most importantly the geometries of the patterns that can be formed on the surface are very limited and are basically constituted by straight lines. Other techniques have been used to fabricate SRGs on azopolymers, such as radially polarized Bessel beam[12] or proximity field nanopatterning.[13]

In this Chapter we employed a confocal microscope to realize precise and complex topographic patterns directly on poly−disperse red 1−methacrylate (pDR1m) substrates. On the contrary to the other techniques described above, confocal microscopes are widely used in most of the laboratories dealing with cell biology, tissue engineering

and biomaterials. Patterns could be drawn onto the pDR1m substrate by controlling the position of the laser beam through the region−of−interest (ROI) editor of the microscope software. Argon laser at both 488 or 514 nm wavelengths was used. As a matter of fact since the maximum absorption band of pDR1m is at 483 nm, both wavelengths were suitable to activate the azobenzene *trans−cis−trans* isomerization, that allowed a macroscopic mass transport in the azo−polymer film. Using this technique we could realize many complex shapes with high spatial control and in few seconds. Additionally many geometries could be embossed on the same support, erased with temperature or unpolarized light and rewritable afterwards for several times. Besides their direct application, patterned azopolymers could be used as masters in replica molding technique, overcoming many practical and economical issues. In fact, soft lithography replica−molding is a well−known and practical technique used to fabricate micro and nano structure[14] with large employment in many fields, such as microfluidics,[15] biochemistry and biology.[16] Silicon masters with a patterned relief structures on their surface are mainly used as molds to replicate their topography on elastomeric materials, despite their realization requires a very costly technique. Thanks to their stability and rigidity, patterned pDR1m azo−polymer films could be used as competitive, low cost and versatile molds. As a proof of concept two well known materials in soft lithography were used to duplicate azopolymer structures, which are PDMS and NOA−63. Moreover, NIH−3T3 response to confocal−induced geometrical patterns was investigated, both in static and in dynamic

way. In fact for the first time, we could dynamically change the surface topography while cells were seeded on the azopolymer substrates.

4.2 Materials and Methods

For substrate preparation, spin coating technique was used in order to realize thin film of pDR1m on cover glasses (700 nm thickness). In details, 12 mm diameter circular cover glasses were washed in acetone, sonicated for 15 min and then dried on a hot plate prior to the spin coating process. pDR1m was dissolved in chloroform at a 5% w/v concentration. The solution was spun over the cover glass by using a Laurell spin coater at 1500 rpm and a profilometer was used to monitor the coated−polymer thickness.

4.2.1 Pattern Realization

A SP5 STED confocal microscope (Leica Microsystems, Germany) was used to emboss different topographic patterns on pDR1m substrates. In more details, the *trans−cis−trans* isomerization of the azopolymer and consequent mass transport were activated by using an Argon laser with either 488 or 514 nm wavelength (1.7 or 2.3 mW maximum intensity, respectively). Patterns were drawn onto the pDR1m substrate by controlling the position of the laser beam through the region−of−interest (ROI) editor of the microscope software. Time exposure was 30 sec.

For surface characterization atomic force microscope (AFM) and scanning electron microscope (SEM) were employed. A JPK NanoWizard II (JPK Instruments, Germany) was used to assess the surface topography of pDR1m films. An Axio Observer Z1 microscope (Zeiss, Germany) was combined to the AFM to control tips and samples. Silicon Nitride tips (MLST, Bruker, USA) with a spring constant of 0.01 N/m were used in contact mode, in air at room temperature. SEM analysis was performed with a Ultra Plus FESEM scanning electron microscope (Zeiss, Germany). Patterned pDR1m samples were mounted on microscope stubs and sputter coated with gold (approximately 7 nm thickness).

4.2.2 Replica molding technique

PDMS and NOA−63 were used to duplicate the confocal−realized patterns with replica−molding technique. PDMS was prepared by mixing elastomer base and curing agent at 10:1 weight ratio. The solution was degassed, poured onto the pDR1m master and then cured at 55°C for 2 h. The PDMS replica was gently peeled off from the mold and examined by AFM. The polyurethane NOA63 was poured onto the pDR1m master as received, squeezed between two clamped glasses and cured for 30 minutes under 365 nm UV light. Temperature was necessary to be able to unmold the polyurethane film from the underlying pDR1m film and the above glass. In order to assess pDR1m master stability after sequential polymer pouring, curing and detaching, multiple replicas were performed on the same master and each of them was characterized with AFM, as previously described.

Pattern features of master and replicas were then compared in order to assess the reproducibility of the technique. In details, pattern height and homogeneity were evaluated.

4.2.3 Cell Culture Experiments

NIH−3T3 fibroblasts were cultured in low glucose DMEM (Dulbecco's Modified Eagle Medium) and incubated at 37°C in a humidified atmosphere of 95% air and 5% CO_2. Patterned pDR1m substrates were sterilized under UV light for 30 minutes and then cells were seeded on them without any additional treatment. After 24 hours cells were fixed with 4% paraformaldehyde for 20 min and then permeabilized with 0.1% Triton X−100 in PBS 1x for 3 min. In order to stain actin filaments with TRITC−phalloidin, samples were incubated for 30 min at room temperature in the phalloidin solution (dilution 1:200). For focal adhesions staining, cells were incubated in a anti−vinculin monoclonal antibody solution (dilution 1:200) for 2 h at 20°C and successively marked with Alexa Fluor 488 conjugated goat anti−mouse antibody (dilution 1:1000) for 30 min at 20°C. Finally cells were incubated for 15 min at 37°C in a ToPro3 solution (dilution 5:1000) to stain cells nuclei. Leica TCS SP5 confocal microscope was used to collect fluorescent images of cells on pDR1m. The laser lines used were 488 nm (vinculin), 543 nm (actin) and 633 nm (nuclei). The emissions were collected in the 500−530 nm, 560−610 nm and 650−750 ranges, respectively.

4.3 Results and Discussion

Single photon confocal microscopy was used to generate submicrometric patterns on azopolymers by tightly controlling the laser beam spatial position, thus enabling the realization of well defined and complex structures. As a matter of fact, most of the confocal software allows to define specific ROIs in which the laser irradiation is active with a high spatial resolution (nm order). A proper wavelength allowed the activation of the azobenzene *trans−cis−trans* isomerization and therefore a macroscopic mass transport in the azo−polymer film. Using this technique, drawing rectangular ROIs and irradiating the sample for 30 seconds with Argon laser at 514 nm wavelength, it was possible to generate easily parallel gratings (Figure 4.1), similar in shape to interference pattern induced for SRGs as shown in Chapter 2.

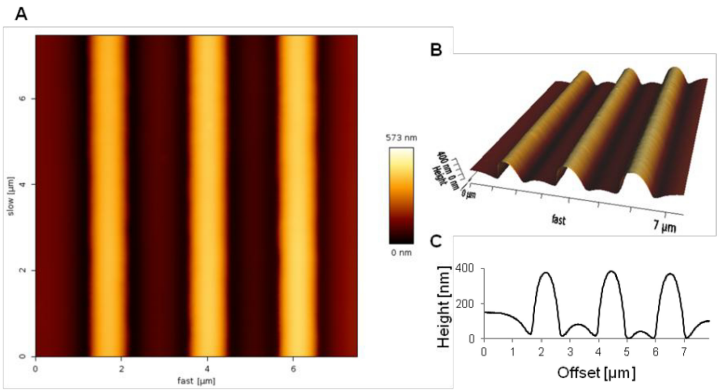

Figure 4.1. AFM image of three lines realized on pDR1m with Argon laser at 514 nm in 30 seconds, (A) bi−dimensional topographical image, (B) three−dimensional image and (C) cross section profile.

The polarized light of the confocal laser beam and the proper wavelength (close enough to 483 nm, that is the maximum absorption band of pDR1m) led the *trans–cis–trans* isomerization of the azobenzene molecules and the consequent polymer mass migration in the direction of the polarized light. By simply changing the shapes of the ROI and dwell time, it was possible to create diverse shapes, like squares, triangles and dots. SEM images of some of the geometries produced with the confocal microscope are shown in Figure 4.2.

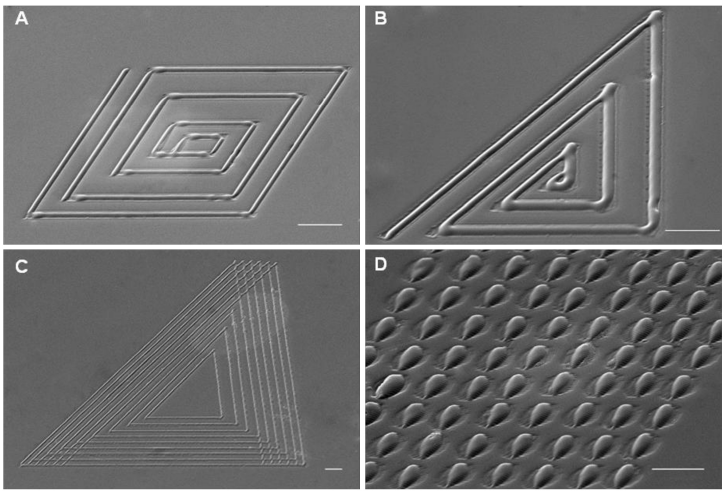

Figure 4.2. SEM images of several patterns realized on pDR1m films by using a confocal microscope, drawing several ROIs and irradiating the sample with 514 nm Argon laser wavelength (2.6 mW intensity). Examples of some confocal–realized patterns: (A) squares, (B–C) triangles and (D) sphere–like geometries. Scale bars are 10 µm.

Remarkably, all of them were impressed on the same substrate, thus demonstrating the versatility of the proposed technique.

Although many mechanisms have been proposed to explain the mass migration phenomenon on azopolymers, the model that suits our

experiments in the best way is the gradient force model.[17,18] According to it, for a cylindrical symmetry light distribution around the propagation axis, like our focused Gaussian laser beam, the mass migration occurs in the direction of the light polarization.[5,19] In this case, the dependence of the driving force $\vec{f}$ from the illuminating electromagnetic field can be synthesized in the relation:

$$\vec{f} \propto [\vec{P} \cdot \vec{\nabla}]\vec{E}$$

where $\vec{E}$ is the electric field and $\vec{P}$ is the local polarizability of the sample.[19] In genaral, a gaussian laser beam induces a material displacement in the direction of the linear polarization of the laser light, with the result of a central groove with two lateral ridges along the light polarization direction.[18] This mass migration along the defined ROIs may be the explanation of the surface elevation encoded on the azopolymer film when irradiated with polarized light.

4.3.1 Relation between Microscope Parameters and Pattern Features

Unlike epifluorescence microscopy, confocal laser microscopy relies on a laser beam that scans the object area in a single− or bi−directional fashion. Therefore, by modulating scanning frequency while maintaining all the other parameters fixed it was possible to control the amount of energy that was transferred to the polymer for each scanning line and hence the extent of maturation. In particular, by drawing rectangular ROIs orthogonal to the scanning direction, we observed the

presence of small fringes on the top of the structures perpendicularly to the pattern direction. Such fringes protruded off 70 nm on 600 nm ridges. Interestingly, fringe periodicity correlates with scanning frequency, in fact by using a scan speed of 100, 200, 400 and 700 Hz the fringe periodicity was 589, 561, 537 and 435 nm, respectively (Figure 4.3). On the base of other reports in literature,[19] we hypothesize that this phenomenon may be due to the material displacement induced by the gaussian laser beam during the scanning process, behaving like a "painting brush".

Conversely, rectangular ROIs, parallel to the scanning direction produced ridges with longitudinal fringes (Figure 4.4).

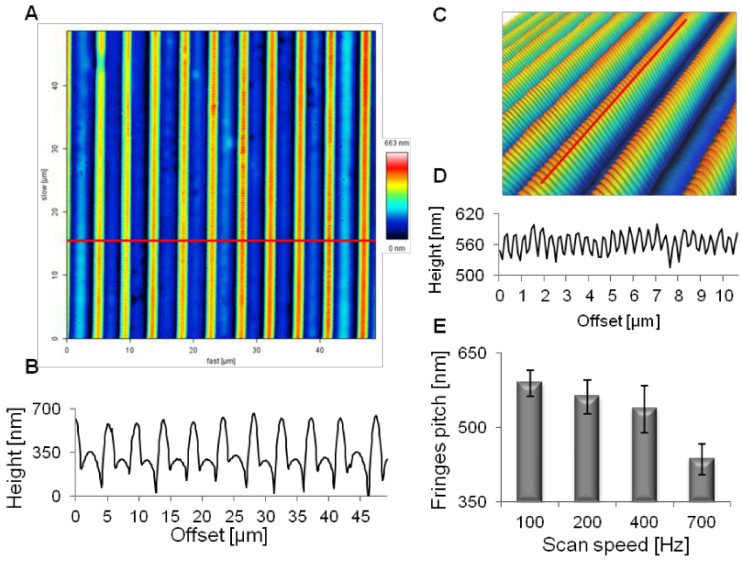

Figure 4.3. (A) AFM height image of a pattern realized on pDR1m drawing the regions of interest orthogonally to the scanner movement, (B) cross−section profile corresponding to the red line in the upper image, (C) three−dimensional image showing small fringes on the top of the ridges, (D) corresponding cross−section and (E) fringe periodicity dependence on the scan speed.

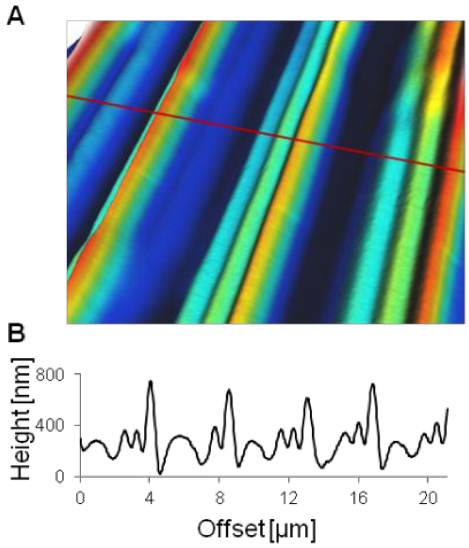

Figure 4.4. (A) 3D AFM image of a pattern realized on pDR1m drawing the regions of interest longitudinally to the scanner movement, (B) cross−section profile corresponding to the red line in the upper image.

On the other hand, by modulating wavelength and laser intensity, while maintaining all the other parameters fixed it was possible to control pattern depth. Argon laser was used at either 488 or 514 nm wavelength and the laser intensity was set at 0.52, 0.91, 1.3 and 1.7 mW. In both cases, increasing the laser intensity it was possible to maximize the depth of the pattern. Moreover, a bigger effect was observed for 488 nm wavelength rater than 514 nm irradiating the samples for 30 sec (Figure 4.5). Actually, the maximum absorption band of pDR1m is at 483 nm, much closer to 488 nm wavelength than to 514 nm. Therefore, with the same irradiation time, the azobenzene molecules were quickly excited at 488 nm wavelength, leading to a faster and more consistent mass migration. Despite we could achieve

patterns with higher features by using 488 nm wavelength, we preferred to use 514 nm one instead. In fact, by aiming to perform experiments with living cells, we preferred to use working conditions with wavelengths less harmful for living systems. As a matter of fact, 514 nm is more distant from UV light, compared to 488 nm, therefore there is an higher probability to let the cells viable after laser irradiation for few seconds.

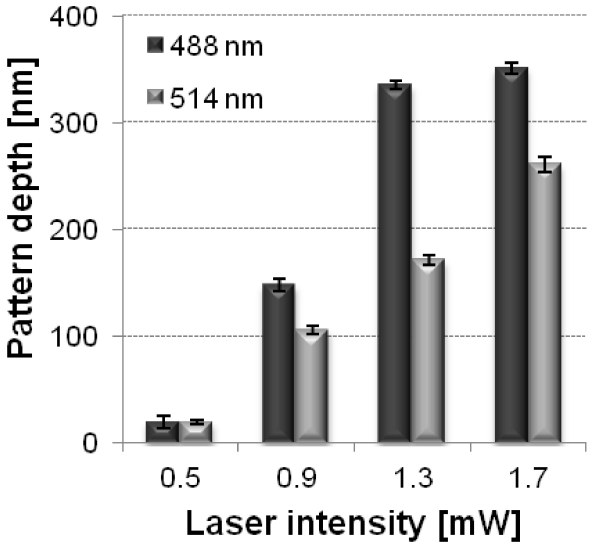

Figure 4.5. Histogram graph showing how to tune the patterns height by modulating laser power and wavelength. Argon laser with 488 or 514 nm wavelength was used at four intensities: 0.52, 0.91, 1.3 and 1.7 mW. Patterns height was measured by AFM, bars refer to standard error of the mean values.

As a proof of concept, in order to eliminate any hypothesis of temperature−induced laser inscription, other wavelengths were tested, such us 633 nm, that is very far from the maximum absorption band of the azopolymer. Indeed, this wavelength left the polymer absolutely

undisturbed and did not allow any embossing effect. One of the many advantages in using and patterning these pDR1m films is that the geometrical features of the imprinted structures proved to be stable at least for more than 6 months if samples were stored in the dark at room temperature. However, pattern erasing process could be intentionally induced by heating the substrates above the glass transition temperature of the polymer (85°C for pDR1m) and new structures could be re−imprinted by further laser expositions.

4.3.2 PDMS and NOA63 Replica Molding

Owing to the adequate stability of the material under specific environmental conditions, we were wondering whether pDR1m could be used as constitutive material for fabricating masters suitable for replica molding. For this reason, parallel arrays of ridges/grooves were created on two pDR1m films. Two different polymers, largely employed in replica molding, namely PDMS and NOA63, were tested. Each polymer was poured on a pDR1m master, cured and detached. Up to 10 replicas were performed on each master and after each procedure; both the master and the replica were characterized by AFM. A graph showing the depth of the topographic features of pDR1m master and replicas is presenting in Figure 4.6.

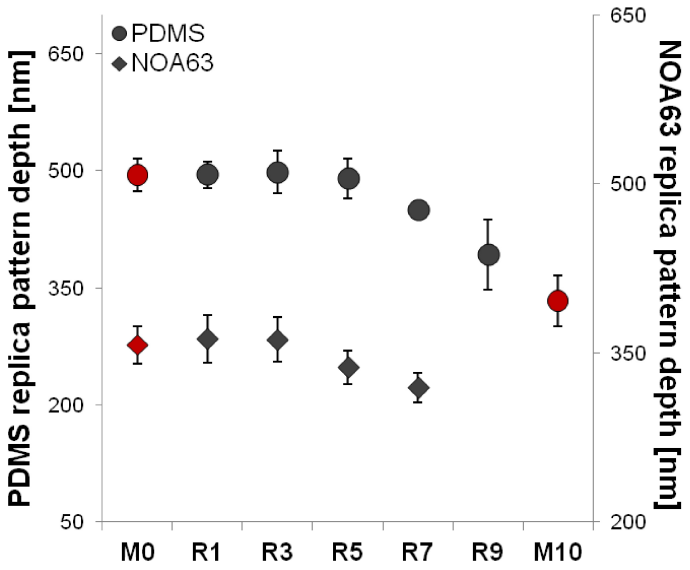

Figure 4.6. Pattern depth of pDR1m master and replica films. PDMS (left axis) and NOA63 (right axis) replica assessment. On the x−axis "M" refer to the master before the process (M0) and after all the replica fabrication (M10), "R" refers to the replicas (R1 to the first replica and so on). Bars represent standard deviations

PDMS replica molding was a really efficient and reproducible process, patterns height was comparable to the master until the fifth replica, thereafter the values of replica depth decreased and the process was less efficient. Regarding NOA−63, the process was very reliable until the third replica, small height reduction occurred from the fifth step and finally the stiff and sticky polyurethane detached completely the master from the underlying glass peeling off the last eighth replica. In wider terms, we can say that replica molding technique with pDR1m master demonstrated to be efficient and the process could be repeated several times, without losing geometrical features, just depth reduction

after the fifth and the third replica for PDMS and NOA63, respectively.

4.3.3 Cell Behavior on Geometrical Patterns

Since a great advantage of these substrates is their biocompatibility, cells can be cultured on them, with no further surface treatments. Therefore, cell behavior, shape and interaction with topography can be studied. Forasmuch as every thinkable pattern can be easily imprinted on the same pDR1m substrate, in a very easy way it is possible to investigate cells expression. For example we could observe that cells could feel and react to different shapes. They were indeed inclined to follow the geometries of our confocal−realized patterns. For example, they tended to be aligned on the linear sides of triangles or the curvatures of concentric rings, on the other hand they were less spread and more roundish on spherical structures (Figure 4.7).

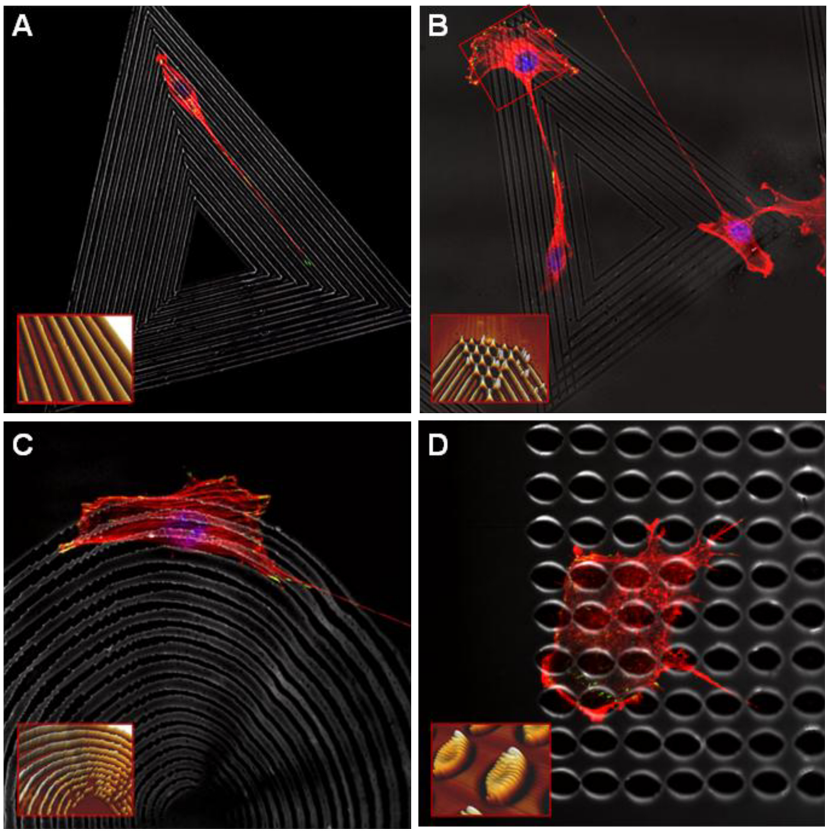

Figure 4.7. Fluorescent images of NIH−3T3 cells on pDR1m confocal−realized patterns. Cells were seeded on triangles patterns, tending to follow the geometry (A) along the sides and (B) on the vertex, (C) on concentric rings and (D) on dots. 3D AFM representations of substrates are shown on the lower left part of each image. Cell cytoskeleton is stained with phalloidin (red), FAs are immunostained for vinculin (green) and nuclei are stained with ToPro3 (blue)

4.3.4 Real−Time Dynamic Cell Guidance

Once demonstrated the versatility of the technique and the biocompatibility of the materials, we were wondering about the possibility to inscribe dynamic patterns in situ, on a cell populated

pDR1m substrate. As a matter of fact, confocal microscopy is provided with a thermo−chamber that allows setting biological conditions, keeping temperature at 37°C and monitoring CO_2. Furthermore, the wavelength of the laser (512 nm) is quite far from harmful UV light, but close enough to the maximum absorption band of the polymer (that is 483 nm), so that it could allow material mass migration, even though leaving cell viable, thanks also to the short exposure time.

In details, cells were cultured on a flat spin coated pDR1m film on cover glass as described above. After 48 hr, the cover glass was fixed with vacuum grease on the bottom of a fluoro−dish and DMEM medium was supplemented with HEPES, in order to control pH.

Once at the microscope, a first confocal image was taken, showing a single cell on flat polymer (Figure 4.8A). Then, after focusing on the material surface, 22 rectangular vertical ROIs were drawn, about 6 μm spaced. 514 nm Argon was shined on the selected regions for 30 sec. The resulting pattern is shown in Figure 4.8B. The cell was apparently undisturbed by the laser inscription and it continued to move changing its own orientation and migrating over the sample. After 45 min of cell monitoring, with the same technique, a second structure was inscribed on the sample, orthogonally to the first one, realizing a grid structure (Figure 4.8C). Once again, cell showed to be viable, moving around the sample and adapting its shape to the new underneath geometries.

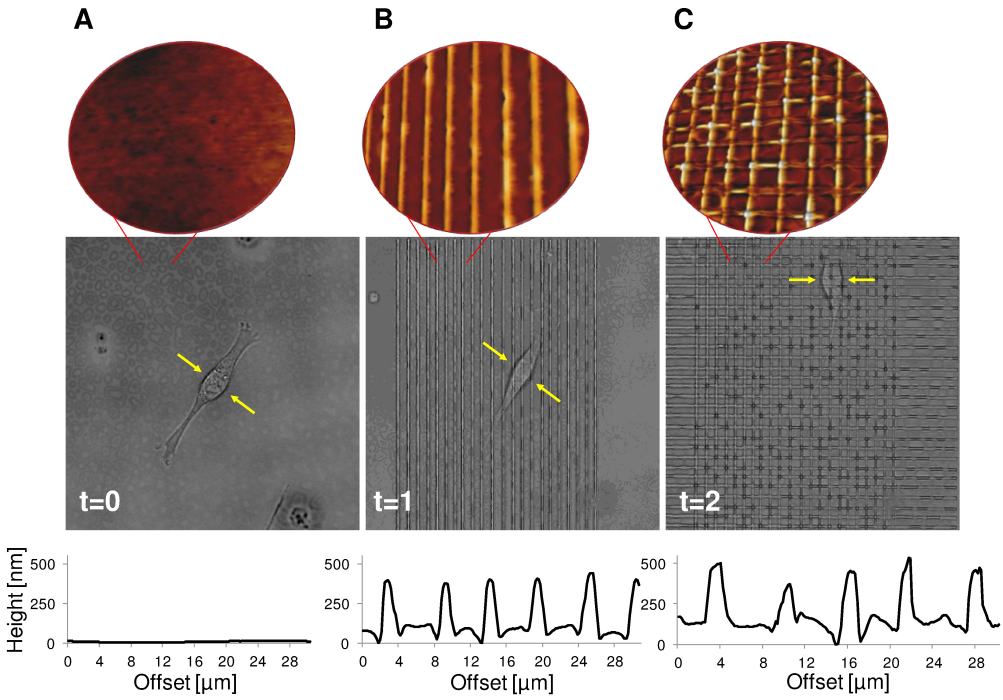

Figure 4.8. In−situ topographic change induced by 514 nm Argon laser (90 µW). Confocal images on (A) single cell on flat pDR1m (t=0), (B) same location after first pattern inscription (t=1) and (C) after second patterning (t=2). Laser exposure was 30 sec each time. On the top and on the bottom part of confocal micrographs, 3D AFM images show topography of substrates and cross−section profiles present pattern dimensions. Yellow arrows show cell nuclear regions.

In order to visualize cell shape and orientation on such realized structures, we decided to reuse the substrate and fix the cells so that we could analyze in details the cytoskeleton assembly and FAs expression. In details, cells were trypsinized, pDR1m substrate was washed with PBS, dried and sterilized under UV. Additional cells were cultured on them, fixed after 24 hr and stained as previously described, in order to

visualize cell cytoskeleton, FAs and nuclei. Figure 4.9 shows confocal micrographs of fixed cells on three different regions of the sample, i.e. flat area, linear pattern realized with confocal single inscription and grid pattern realized with two subsequent orthogonal inscriptions. Cells were randomly oriented on flat region (Figure 4.9A), conversely they were more elongated on linear pattern (Figure 4.9B) and again randomly oriented on the grid (Figure 4.9C). Remarkably, higher concentration of FAs could be visualized on flat polymer thus demonstrating the cell ability to develop FAs on a isotropic substrates with respect to patterned surfaces.[20] This experiment is in agreement with many reports in literature regarding cell behavior on topographic pattern[21–23] and with the results of cell orientation on linear and grid patterns, showed in Chapter 2.

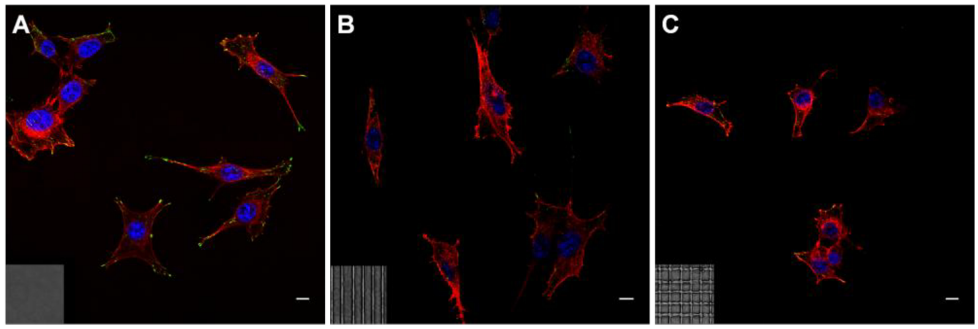

Figure 4.9. Confocal images of fixed NIH−3T3 cultured on (A) flat pDR1m, (B) confocal−realized linear pattern and (C) double pattern inscription with confocal. Cell cytoskeleton is stained with phalloidin (red), FAs are immunostained for vinculin (green), nuclei are stained with ToPro3 (blue).

Moreover, this experiment showed how patterns realized during the real−time observation (Figure 4.8) could actually influence cell behavior and response after 24 hr from cell seeding.

Taking together all these experiments may pave the way to a dynamic and programmable use of azopolymer substrates for cell culture in real−time, showing the possibility to introduce a new kind of cell−instructive materials. In this way, topographic signals may be modulated any time and cell behavior could be studied accordingly. This approach has the advantage to be dynamic and adjustable, due to cell culture supports that are switchable on−demand. This gives rise to study cell behavior in a more biomimetic way. As a matter of fact, in Nature, extra−cellular matrix is continuously changing its own features, presenting anytime different signals to local cells, hence influencing their behavior and determining cell fate.

4.4 Conclusions

In this chapter, we have presented an innovative technique to inscribe patterns on azopolymers. Confocal microscopy is widely present in all the laboratories dealing with cells and it allows a tightly control of laser positioning and therefore pattern inscription. By using this instrumentation, complex and multiscale patterns can be imprinted on spin−coated supports in few seconds and they are stable for months.

The potential uses of such structured substrates in science are many, from micro−fabrication to cell culture. As a matter of fact, patterned azopolymers proved to be efficient, low cost and easy−to−fabricate masters in replica molding technique. Additionally, owing to their

biocompatibility, cell could be seeded on them without any additional treatments.

Remarkably, we demonstrated for the first time that this patterning technique is perfectly adaptable for dynamic cell guidance experiments. Pattern could be imprinted several times on a cell populated azopolymer support, influencing cell response without compromising cell viability.

Taken together these findings demonstrate that the proposed technique may have a great impact in many research fields. Above all, this study could pave the way to the use of new class of cell−instructive biomaterials that can present topographic signals on−demand hence allowing to investigate and unravel many processes involved in cell−topography interaction. In fact, this interaction has proved to be a key factor when designing a new material for tissue engineering.

4.5 References

(1) Cojocariu, C.; Rochon, P. Light−induced motions in azobenzene−containing polymers. *Pure Appl. Chem.* **2004**, *76*, 1479−1497.
(2) Natansohn, A.; Rochon, P. Photoinduced motions in azo−containing polymers. *Chem. Rev.* **2002**, *102*, 4139−4176.
(3) Seki, T.; Fukuda, K.; Ichimura, K. Photocontrol of polymer chain organization using a photochromic monolayer. *Langmuir* **1999**, *15*, 5098−5101.
(4) Barrett, C.; Natansohn, A.; Rochon, P. Cis−trans thermal isomerization rates of bound and doped azobenzenes in a series of polymers. *Chem. Mater.* **1995**, *7*, 899−903.
(5) Rochon, P.; Batalla, E.; Natansohn, A. Optically induced surface gratings on azoaromatic polymer films. *Appl. Phys. Lett.* **1995**, *66*, 136−138.
(6) Kim, D.; Tripathy, S.; Li, L.; Kumar, J. Laser-induced holographic surface relief gratings on nonlinear optical polymer films. *Appl. Phys. Lett.* **1995**, *66*, 1166−1168.
(7) Marder, S. R.; Kippelen, B.; Jen, A. K.−Y.; Peyghambarian, N. Design and synthesis of chromophores and polymers for electro−optic and photorefractive applications. *Nature* **1997**, *388*, 845−851.
(8) Priimagi, A.; Shevchenko, A. Azopolymer-based micro-and nanopatterning for photonic applications. *J. Polym. Sci. Pol. Phys.* **2014**, *52*, 163−182.
(9) Barillé, R.; Janik, R.; Kucharski, S.; Eyer, J.; Letournel, F. Photo−responsive polymer with erasable and reconfigurable micro− and nano−patterns: an in vitro study for neuron guidance. *Colloids Surf., B* **2011**, *88*, 63−71.
(10) Rocha, L.; Păiuş, C.−M.; Luca−Raicu, A.; Resmerita, E.; Rusu, A.; Moleavin, I.−A.; Hamel, M.; Branza−Nichita, N.; Hurduc, N. Azobenzene based polymers as photoactive supports and micellar structures for applications in biology. *J. Photoch. Photobiol. A* **2014**, *291*, 16−25.
(11) Baac, H.; Lee, J.−H.; Seo, J.−M.; Park, T. H.; Chung, H.; Lee, S.−D.; Kim, S. J. Submicron−scale topographical control of cell growth using holographic surface relief grating. *Mat. Sci. Eng. C* **2004**, *24*, 209−212.
(12) Grosjean, T.; Courjon, D. Photopolymers as vectorial sensors of the electric field. *Opt. Express* **2006**, *14*, 2203−2210.
(13) Lambeth, R. H.; Park, J.; Liao, H.; Shir, D. J.; Jeon, S.; Rogers, J. A.; Moore, J. S. Proximity field nanopatterning of azopolymer thin films. *Nanotechnol.* **2010**, *21*, 165301.

(14) Xia, Y.; Whitesides, G. M. Soft lithography. *Annu. Rev. Mater. Sci.* **1998**, *28*, 153−184.
(15) Kim, P.; Kwon, K. W.; Park, M. C.; Lee, S. H.; Kim, S. M.; Suh, K. Y. Soft lithography for microfluidics: a review. *BioChip J.* **2008**, 1−11.
(16) Whitesides, G. M.; Ostuni, E.; Takayama, S.; Jiang, X.; Ingber, D. E. Soft lithography in biology and biochemistry. *Annu. Rev. Biomed. Eng.* **2001**, *3*, 335−373.
(17) Kumar, J.; Li, L.; Jiang, X. L.; Kim, D.−Y.; Lee, T. S.; Tripathy, S. Gradient force: the mechanism for surface relief grating formation in azobenzene functionalized polymers. *Appl. Phys. Lett.* **1998**, *72*, 2096−2098.
(18) Bian, S.; Liu, W.; Williams, J.; Samuelson, L.; Kumar, J.; Tripathy, S. Photoinduced surface relief grating on amorphous poly (4−phenylazophenol) films. *Chem. Mater.* **2000**, *12*, 1585−1590.
(19) Ambrosio, A.; Camposeo, A.; Carella, A.; Borbone, F.; Pisignano, D.; Roviello, A.; Maddalena, P. Realization of submicrometer structures by a confocal system on azopolymer films containing photoluminescent chromophores. *J. Appl. Phys.* **2010**, *107*, 083110.
(20) Yim, E. K.; Darling, E. M.; Kulangara, K.; Guilak, F.; Leong, K. W. Nanotopography−induced changes in focal adhesions, cytoskeletal organization, and mechanical properties of human mesenchymal stem cells. *Biomaterials* **2010**, *31*, 1299−1306.
(21) Natale, C. F.; Ventre, M.; Netti, P. A. Tuning the material−cytoskeleton crosstalk via nanoconfinement of focal adhesions. *Biomaterials* **2014**, *35*, 2743−2751.
(22) Ventre, M.; Natale, C. F.; Rianna, C.; Netti, P. A. Topographic cell instructive patterns to control cell adhesion, polarization and migration. *J. Roy. Soc. Interface* **2014**, *11*, 20140687.
(23) Biela, S. A.; Su, Y.; Spatz, J. P.; Kemkemer, R. Different sensitivity of human endothelial cells, smooth muscle cells and fibroblasts to topography in the nano–micro range. *Acta Biomater.* **2009**, *5*, 2460−2466.

Conclusions and Future Prospects

The research described in this thesis aimed to introduce a new class of cell–instructive materials, designed to study cell response to dynamic topographic signals.

Understanding cellular reaction to the external environment is a central aspect in tissue engineering and biomedical science. A growing number of works is emphasizing the high sensitivity that cells display towards the chemical and physical features of the substrate to which they are connected. In particular, substrates of defined topography have emerged as powerful tools in the investigation of the mechanisms involved in cell–material interaction. The limitation of many of the proposed substrates is their static form, which does not allow to induce a programmed change during cell culture. This physical stasis has limited the potential of topographic substrates to control cells in culture. For this reason a study on dynamic and reversible platforms was conducted, aiming to investigate cell behavior in a more biomimetic way and to overcome the limit of static systems.

In **Chapter 1** an overview of cell–material interaction, azopolymers and their biological applications is given.

In **Chapter 2** an effective technique to imprint and modify biocompatible topographic patterns on azopolymer coated glass, using conventional optical equipments, was presented. Patterned substrates in the forms of linear gratings (2.5 and 5.5 μm pitch) or grid structure

(2.5 × 2.5 μm) were inscribed on poly−Disperse Red 1−methacrylate (pDR1m) films. Such topographies proved to be effective in confining focal adhesion (FA) growth and cytoskeletal assembly. In fact NIH−3T3 fibroblasts were elongated and polarized in the direction of linear patterns and randomly oriented on flat controls and grid structures. Patterns could be easily erased and rewritten in dry conditions, whereas in a wet environment circularly polarized or incoherent light were able to alter pattern shape. In particular, incoherent and unpolarized light−mediated erasure proved to be a promising strategy for real−time experiments with living cells as microscopy set−up and illumination exposure time did not affect cell viability. In fact, we could irradiate a cell populated 2.5 μm linear pattern with a mercury lamp, implemented in a confocal microscopy, erasing the pattern and changing the surface topography, while cells were still vital and migrated along the substrate. Therefore, the system we proposed had the potential to be employed for understanding cell behavior and possibly mechanotransduction events in a dynamic environment.

In the field of cell−material interaction, cell elasticity is a fundamental parameter that reflects the state of a cell. Even though topographic cues proved to be a powerful tool to control different aspects of the cell behavior, the literature concerning the effects of topographies on cell mechanics is relatively scarce. In **Chapter 3** we showed that micropatterned substrates strongly influence cell mechanical properties along the whole cell body, from peripheral regions up to the nuclei, apart from morphology, as shown in the previous chapter. In particular, we found that fibroblasts cultured on 2.5 and 5 μm linear patterns

possessed significantly stiffer bodies and nuclei, in comparison to those cultured on isotropic flat controls or grid patterns (2.5 × 2.5 grid). Since actin cytoskeleton is known to play a critical role in determining cell mechanical properties and is physically connected to cell nuclei we investigated cytoskeleton assemblies and nuclei morphology to gain a better insight into the material−cytoskelton crosstalk. Primarily, we found that the elastic properties of the cell body were directly proportional to those of cell nuclei. Moreover, a connection between cell nuclei mechanical proprieties and morphology was found. In fact, in comparison with cell nuclei on flat controls, cell nuclei on linear patterns showed an higher aspect ratio, a lower volume and stiffer values of Young's moduli. In other words, highly elongated cells, as those on the 2.5 μm and 5 μm linear pattern, possessed oblong and smaller nuclei that were also the stiffest ones. Our work proved that topographic signals can be used as critical tools to control and direct mechanical properties of cells. This result may become useful in the development of new cell−instructive biomaterials for tissue engineering.

In **Chapter 4**, we presented a new technique to inscribe patterns on azopolymers. Confocal microscopy is widely present in all the laboratories dealing with cells and it allows a tightly control of laser positioning and therefore pattern inscription. By using this instrumentation, complex, multiscale and stable patterns could be imprinted on spin−coated pDR1m films in few seconds. The potential use of such structured substrates in research is extended, from microfabrication to cell culture. As a matter of fact, patterned azopolymers proved to be efficient, low cost and easy−to−fabricate

masters in replica molding technique. Additionally, owing to their biocompatibility, they could be used as cell culture supports. Remarkably, we demonstrated for the first time that this patterning technique is perfectly adaptable for dynamic cell guidance experiments. Pattern could be imprinted several times on a cell populated azopolymer support, influencing cell response. Interestingly, cell viability was not influenced.

Taken together these findings demonstrate that the proposed technique may have a great impact in many research fields. Above all, this study could pave the way to the use of a new class of cell−instructive biomaterials, on which topographic cues can be presented on−demand hence allowing to unravel many processes involved in dynamic cell−topography interaction.

List of Publications

Ventre, M.; Natale, C. F.; **Rianna, C.**; Netti, P. A. Topographic Cell Instructive Patterns to Control Cell Adhesion, Polarization and Migration. *J. Roy. Soc. Interface* **2014**, *11*, 20140687.

Submitted Manuscript:

Rianna, C.; Calabuig, A.; Ventre, M.; Cavalli, S.; Pagliarulo, V.; Grilli, S.; Ferraro, P.; Netti, P. A. Reversible Holographic Patterns on Azopolymers for Guiding Cell Adhesion and Orientation.

Manuscripts in Preparation:

Rianna, C.; Ventre, M.; Cavalli S.; Radmacher M.; Netti P. A. Micropatterns Regulate Cell Mechanics through the Material−Cytoskeleton Crosstalk.

Rianna, C.; Kollarigowda, R. H.; Ventre, M.; Cavalli, S.; Netti, P. A. Pattern Realization on Azopolymers by using Confocal Microscope: a Fast Technique for Replica−Molding and Cell Culture Applications.

Kollarigowda, R. H.; De Santo, I.; **Rianna, C.**; Manikas, A.; Cavalli, S; Netti, P. A. Shedding Light on Azopolymer Brush Mobility by Fluorescence Correlation Spectroscopy.

Appendix

Influence of Material Stiffness on Cell Mechanics

Abstract. Mechanical properties of cells and extracellular matrix (ECM) play important roles in many biological processes including stem cell differentiation, tumor formation, and wound healing. Changes in stiffness of cells and ECM are often signs of changes in cell physiology or diseases in tissues. Hence, cell stiffness is an index to evaluate the status of cell cultures. Among the multitude of methods applied to measure the stiffness of cells and tissues, micro−indentation using an Atomic Force Microscope (AFM) provides a way to measure the stiffness of living cells. In this Appendix a study of cell mechanics on different stiffness substrates by AFM is reported. Polyacrylamide (PAA) gels were realized tuning their stiffness by varying the ratio between the acrylamide and the cross−linker bisacrylamide. Cells were seeded on these gels, then cell mechanical properties were measured and connected to each stiffness−tuned support.

The work presented in this Appendix has been performed at the Biophysics Institute−University of Bremen, under the supervision of Prof. Manfred Radmacher.

The mechanical properties of the extracellular matrix (ECM) contribute to the regulation of many important cell processes that determine cell fate and function.[1] Within the body, the stiffness of several cell microenvironments display high variation. In fact, between different tissues, extracellular matrix rigidity often varies over several orders of magnitude, e.g., brain (260–490 Pa), liver (640 Pa), kidney (2.5 kPa), skeletal muscle (12–100 kPa) and cartilage (950 kPa).[2] Moreover, local stiffness can vary strongly, giving rise to complex rigidity gradients that can span several orders of magnitude, such as those noted at interfacial tissues.[3] For these reasons, the study of cell mechanics on materials with a wide range of stiffness values may have an important role for creating favorable conditions when designing new biomaterials and unravel cell processes throughout variation of local stiffness.

In this work we studied cell mechanical properties in response to different stiffness substrates. The aim of the study was comparing the viscoelastic properties of cells spread on materials with elasticity modulus ranging from 200 to 40,000 Pa under the same biochemical conditions. Polyacrylamide (PAA) was chosen as a suitable material to carry out the experiments. This allowed us to tune the elastic properties by changing the concentration of monomer and/or cross−linker in the pre−polymer solution. In fact, by changing the concentration of bisacrylamide it was possible to realize gels with different elastic modulus values. PAA gels were covalently bound to amino−silanated cover glasses and used as cell culture support. Visco−elastic properties of NIH−3T3 fibroblasts, spread on PAA gels with different stiffness values were investigated by using an atomic force microscope (AFM).

In details, a MFP3D AFM (Asylum Research) was used to measure the topography and mechanical properties of cells. An optical microscope was combined to the AFM to be able to control tips and sample. Soft cantilevers (Bio−MLCT, Bruker, nominal spring constant 0.01 Nm^{-1}) were used to investigate cell properties.

As previously mentioned, PAA is a gel that permits to tune the stiffness values by adjusting monomer and cross−linker ratio. In this way the surface chemistry can be considered constant, while changing mechanical properties. The basic recipe used for gel realization is shown in Table 1.

Chemicals	Amounts
Milli−Q water	7.87 ml
40% Acrylamide	1.87 ml
2% Bisacrylamide	200 µl
10% APS	50 µl
TEMED	5 µl

Table 1. Chemical amounts used to realize PAA gels. With these concentrations the resulting gel had a stiffness of ~10 kPa.

Glass cover slides were primarily treated with a silanization process in order to attach PAA gels covalently on them, as previously reported.[3] Such process consisted in incubating cover slides in a NaOH (sodium hydroxide) solution, followed by addition of 3−APTMS (*N*−[3−(Trimethoxysilyl)propyl]ethylenediamine). Glutaraldehyde was then used to cross−link the 3−APTMS on the glass slides and the PAA

gel. Force maps, by meaning of grid of multiple force curves, were executed on these gels as well as on the cells cultured on them. In details, mechanical properties of stiff and soft samples, in terms of Young's moduli or elastic moduli (E) were estimated from each force curve within a force map. Evaluation was performed with the date analysis package IGOR (Wavemetrics). The Hertzian model was used to calculate Young's modulus from every force curve. Elastic moduli of tuned−stiffness PAA gels are showed in Figure 1.

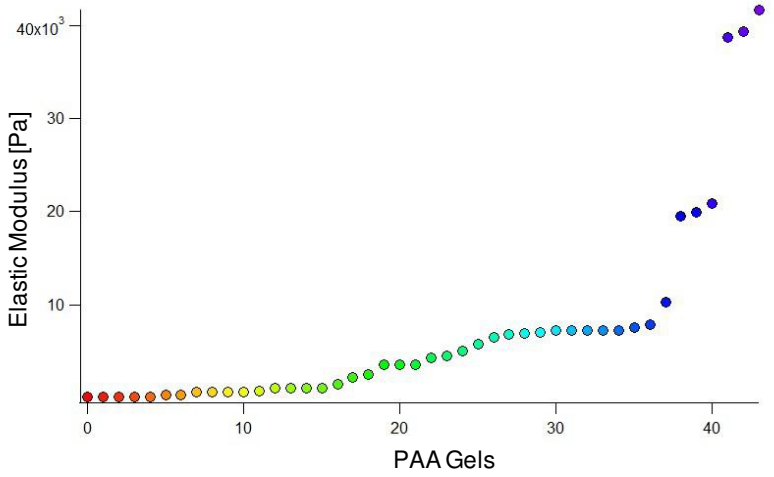

Figure 1. Elastic moduli of PAA gel samples. Each marker represents the median value of all the elastic moduli extracted from each force curve within a force map.

Such force maps were performed on cells cultured on PAA substrates as well and therefore an eventual relationship between elasticity of cells and gels was investigated. We found that cell mechanical properties (ECell) were directly related to substrate stiffness (EGel). In fact cell stiffness (or softness in this case) ranged between 200 Pa on

the softest gels and increased up to 3000 Pa, when the gel stiffness was 10kPa or larger (Figure 2). Therefore, ECell followed a power law, i.e. it was proportional to EGel.

For EGel values above 10kPa, ECell reached a kind of stable saturation, in this case cell stiffness values are comparable to those obtained for cell seeded on a typical cell culture stiff substrate (such us glass or polystyrene).

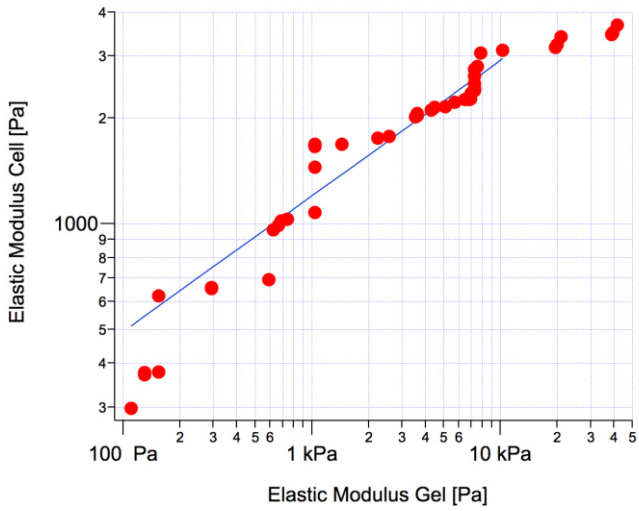

Figure 2. Elastic moduli of cells versus elastic moduli of PAA gels. A positive dependency was found. Red circles indicate median values of elastic moduli extracted from each force map.

Cell culture supports proved to influence largely cell behavior. In fact, Sunyer et al.[4] found that cell spreading on hydrogels linearly depends on hydrogel stiffness. Other reports showed that cell morphology, adhesion and cytoskeleton structure are influenced by material stiffness.[5, 6] Moreover, the actin cytoskeleton is known to play a central

role in determining mechanical properties of cells.[7,8] Therefore, it is tempting to speculate that as there is a dependency between cytoskeleton organization and mechanical properties of substrates, cell mechanical properties show this direct dependency as well.

References

(1) Discher, D. E.; Janmey, P.; Wang, Y.−l. Tissue cells feel and respond to the stiffness of their substrate. *Science* **2005**, *310*, 1139−1143.
(2) Levental, I.; Georges, P. C.; Janmey, P. A. Soft biological materials and their impact on cell function. *Soft Matter* **2007**, *3*, 299−306.
(3) Seidi, A.; Ramalingam, M.; Elloumi−Hannachi, I.; Ostrovidov, S.; Khademhosseini, A. Gradient biomaterials for soft−to−hard interface tissue engineering. *Acta biomater.* **2011**, *7*, 1441−1451.
(4) Sunyer, R.; Jin, A. J.; Nossal, R.; Sackett, D. L. Fabrication of hydrogels with steep stiffness gradients for studying cell mechanical response. *PloS One* **2012**, *7*, e46107.
(5) Cretu, A.; Castagnino, P.; Assoian, R. Studying the effects of matrix stiffness on cellular function using acrylamide−based hydrogels. *J. Visualized Exp.* **2010**.
(6) Yeung, T.; Georges, P. C.; Flanagan, L. A.; Marg, B.; Ortiz, M.; Funaki, M.; Zahir, N.; Ming, W.; Weaver, V.; Janmey, P. A. Effects of substrate stiffness on cell morphology, cytoskeletal structure, and adhesion. *Cell Motil. Cytoskeleton.* **2005**, *60*, 24−34.
(7) Moeendarbary, E.; Valon, L.; Fritzsche, M.; Harris, A.R.; Moulding, D.A.; Thrasher, A.J.; et al. The cytoplasm of living cells behaves as a poroelastic material. *Nat. Mater.* **2013**,*12*, 253−61.
(8) Rotsch, C.; Radmacher, M. Drug−induced changes of cytoskeletal structure and mechanics in fibroblasts: an atomic force microscopy study. *Biophys. J.* **2000**,*78*, 520−35.

Acknowledgments

I will write my acknowledgments in Italian and some in English to make sure that my gratitude reaches all people as clearly as possible.

Vorrei ringraziare tutte le persone che hanno reso possibile la realizzazione di questa tesi di dottorato e hanno supportato la mia attività durante questo meraviglioso percorso formativo.

Prima di tutto vorrei esprimere la mia gratitudine al Prof. Paolo A. Netti, dapprima stimato docente universitario, poi relatore della tesi specialistica ed infine tutor del mio dottorato. Vorrei ringraziarlo per avermi dato la possibilità di crescere professionalmente e coltivare la mia passione per la ricerca scientifica in un ambiente stimolante e multidisciplinare, seguendo il mio lavoro con passione ed entusiasmo.

Senza il supporto ed i preziosi consigli dei miei due fantastici co-tutor, il mio percorso di dottorato non sarebbe stato uguale e di certo non così gratificante ed entusiasmante. Pertanto ringrazio immensamente la Dott.ssa Silvia Cavalli e il Prof. Maurizio Ventre per il supporto scientifico e personale che mi hanno dato durante questi tre anni. La loro esperienza mi ha guidato durante questo percorso e non bastano parole per ringraziarli per tutto ciò che mi hanno insegnato, per la dedizione, la professionalità e il rigore scientifico che mi hanno trasmesso.

Inoltre estendo i miei ringraziamenti al Prof. Pietro Ferraro, al Dr. Vito Pagliarulo e ad Alejandro Calabuig (CNR−Istituto di Cibernetica "E. Caianiello"), con i quali ho potuto collaborare durante questi anni e che hanno reso possibile la realizzazione di molti esperimenti descritti nel Capitolo 2 di questa tesi.

During two visits to the Institute for Biophysics in Bremen I was able to improve my knowledge about atomic force microscopy (AFM) for biological applications, under the supervision of Professor Manfred Radmacher. Most of the work presented in Chapter 3 and Appendix

has been performed there. For this reason I would like to thank Prof. Radmacher and all his group for giving me the opportunity to learn a lot about the field of biophysics and cell mechanics. Above all I wish to thank Holger Doschke for supporting me in the AFM data analysis.

Altre persone, altrettanto importanti per il mio dottorato meritano la mia enorme gratitudine. Pertanto ringrazio il Dr. Carlo Natale, mio "maestro cellulare", nonché grande amico e stimato collega, per avermi trasmesso delle conoscenze fondamentali nell'ambito degli studi biologici. Ringrazio inoltre il Dr. Manlio Colella e il Dr. Fabio Formiggini per avermi introdotto nel mondo della microscopia a forza atomica e confocale rispettivamente. Per entrambi riservo un'immensa stima, sia professionale che personale.

Furthermore, I need to thank all the collegues of the Itialian Institute of Technology of Naples (Center for Advanced Biomaterials for Healthcare), above all my "deskmate" Nunzia Di Luise and the members of my research group, the "magic team", for sharing with me the best and the worst moments of our PhD: Ravichandran Kollarigowda, Elisa Vaselli and the new members of the team: Chiara Fedele and Lucia Rossano for their experimental support in last weeks of my PhD.

Infine ringrazio la mia famiglia per il costante sostegno.

With an AFM image, from the bottom of my heart, I want to say to all of you: